Analysis of local circuit of the superior colliculus using multielectrode stimulating/recording system

Penphimon Phongphanphanee

DOCTOR OF PHILOSOPHY

Department of Physiological Sciences

School of Life Science

The Graduate University for Advanced Studies

2008

Analysis of local circuit of the superior colliculus using multielectrode stimulating/recording system

Penphimon Phongphanphanee

DOCTOR OF PHILOSOPHY

Department of Physiological Sciences

School of Life Science

The Graduate University for Advanced Studies

2008

Abstract

The main goal of our study is to clarify the neuronal connection and signal processing within the local circuit of SC. We have introduced the new planar multi-electrode stimulating/recoding system that deals with the populations of neurons to overcome the previous limitation of one-directional recording. This system records field potential simultaneously from 64 locations, 8x8 array with 150 μm inter-electrode space. Moreover, while recording the field potentials in slice, it is possible to perform whole-cell patch-clamp recording simultaneously. The interlaminar and intralaminar circuits of the SC are described in this paper. The spread of activity from the stimulation in the superficial layers indicates the existence of visuomotor pathway. The signal arisen in the sSC propagated in non-linear amplification, particularly in the dSC. The large area of propagation covering almost entire dSC area shows that the motor vector occurring in the dSC preceding the orienting movement recruits a large population of dSC neurons, while the center of mass is moving ventrally. Interestingly, it is found that the dSC stimulation evoked the less spreading burst than that evoked by the sSC stimulation. Furthermore, the spontaneous bursts, proposed to share the basic mechanism with the presaccadic burst in the dSC, always originally occur in the sSC, and disappear when the I_h blocker was applied.

In the lateral connection in the sSC, the horizontal slice comprising SGS and SO layer was tested. The SGS neurons were recorded by the whole-cell patch-clamp, while stimulations were initiated in the SO layer in the opposite side of slice. This method can preserve more the lateral circuit than the coronal or parasagittal slices. Using this new experimental model, the distant inhibitory connection in SGS layer is showed clearly. The distant inhibition and nearby excitation are the basic concept of many computational model of attention.

Contents

Part I

General Introduction

The sensorimotor integration process in the brain is one of the general interests to many neurobiologists. A sudden stimulus usually triggers responses that orient the eyes, ear pinnae, head or body toward the direction of the stimulus. Such orienting behavior requires fast translation of sensory signals to motor commands to initiate new movement or modify ongoing one.

It is believed that the superior colliculus (SC), a brainstem center that converges the sensory input to motor command, plays a crucial role in for the control of goal directed orientating responses towards novel sensory stimuli. The SC is a laminated structure divided on the anatomical ground into seven alternating cellular and fibrous layers from dorsal to ventral (Huerta and Harting, 1984). These seven layers form two major functional divisions: (i) superficial layers (sSC) including *stratum zonale* (SZ), *stratum griseum superficiale* (SGS) and *stratum opticum* (SO); (ii) deeper layers (dSC) including *stratum griseum intermediale* (SGI), *stratum album intermediale* (SAI) and *stratum griseum profundum* (SGP). While the sSC receives the exclusively visual information from the retina and visual cortex, the dSC receives non-visual information from many brain regions and send motor command to the brainstem gaze centers (May, 2006).

During the last several decades, a voluminous literature related to the structure and function of the SC have been published (Sparks, 1986). However, a great attention has been directed toward understanding the afferent and efferent connections of the SC, but surprisingly, the intrinsic circuit organization of this structure is poorly understood.

In this work, the neuronal connectivity and signal processing of the SC local circuit has been investigated at the synaptic level in slice preparations obtained from the mouse. We have introduced a new experimental stimulating/recording system for analysis of the activity of a large population of neurons, to overcome the problems due to sparse samplings from a small number of cells in case of whole-cell patch-clamp recording studies, or recording from a small number of recording tracks in case of field potential recording experiments.

This paper consists of three parts:

Part II, Spatio-temporal profiles of field potentials in the mouse SC slices

Part III, Generation of synchronous burst activity in the intermediate layer

Part IV, The lateral connections in the superficial layer

The spread of activity from the sSC to the dSC was analyzed to reveal the neuronal connections in the SC slices and the signal propagation through the intrinsic visuomotor pathway in **Part II**. In normal controls, the excitatory field responses, shown as negative potential, were restricted to the electrodes adjacent to the stimulation of the sSC, and no clear responses were observed in the dSC. In contrast, when the $GABA_A$ receptor antagonist was applied, a large and long lasting negative response was evoked in the dSC that followed a positive potential. We demonstrated that the activation zone of such stimulation spreads more than 1 mm in the horizontal direction and its center gradually shifts from the dorsal to ventral portion of the dSC. The field potentials were then simultaneously recorded with the whole-cell patch-clamp to clarify the relationship

between these two recording systems. Finally, we have confirmed the field responses in our finding by the uncaging glutamate photostimulation system.

In **Part III**, we submerged the SC slice in the extracellular solution, containing low concentration of Magnesium and 10 μM bicuculline. Under this condition, spontaneous bursts were induced in both field and whole cell recording system. These spontaneous activities are proposed to share common mechanisms with presaccadic burst activity in SGI neurons. This condition was used to study the mechanism underlying the generation of synchronous burst in the dSC. The spontaneous activities in all 64-channel exhibited the similar pattern to the burst that evoked by electrical stimulation. We have tested the hypothesis that the wide field vertical cells, a specific cell type located in the ventral portion of the sSC, are the origin of propagation of spontaneous bursts.

Then, we have changed to use the horizontal slices, instead of coronal or parasagittal slices, to study the role of the SC in the competitive process for saliency among different locations in the visual field in **Part IV**. We have introduced a new *in vitro* experiment in which the lateral connections are preserved in the sSC, horizontal slices, and stimulations are applied in systematically varied locations. The horizontal slice comprised of SGS and SO layers was placed on the array of microelectrodes with the SO-side attached to the planar electrodes. We expected that with this arrangement, optic fibers innervating each location of the sSC are selectively stimulated. The excitatory postsynaptic potential (EPSP) or inhibitory postsynaptic potential (IPSP) in the SGS neurons, elicited by stimulations of one of the planar electrodes, were recorded with whole-cell patch-clamp recording. We analyzed the responses from electrodes arranged in rostrocaudal and lateromedial directions and found that the response properties

depended on the distances between the stimuli and the neurons. We tested two ways of stimulus protocols, single pulse and multiple pulses. The "excitatory center-inhibitory surround" competitive interaction was found clearly in the high frequency repetitive stimulus condition. Furthermore, the neural network mediating the close excitatory and distant inhibitory connections was investigated in the voltage clamp recording. Both excitatory and inhibitory networks have both short- and long-range connections and they are overlapped, but the area of inhibition tended to be larger than that of excitation. We conclude that the different temporal patterns of excitatory and inhibitory connections, at least partially, mediate their competitive relationship.

Part II

Spatio-temporal profiles of field potentials in the mouse SC slices

Introduction

The long-history question of weather or not there is communication between neurons in the sSC and the dSC has been gradually answered. The existence of the visuo-motor pathway between these two layers has been proven in *in vitro* slice experiment (Lee et al., 1997; Isa et al., 1998; Özen et al., 2000; Saito and Isa, 2003). The anatomical data in many species including human (Tardif et al, 2005) also support the hypothesis that the intrinsic connection from neurons in the sSC to the dSC provide a route that visual input can access the premotor neuron in the intermediate layer (SGI).

Many works devoted to clarify the mechanism underlying the interlaminar connections in the SC. The in vitro studies did show that single pulse stimulation of the sSC induces weak or no synaptic responses in the dSC neurons, while the same stimulation induces strong bursting spike responses and long lasting depolarization in dSC neurons when $GABA_A$-mediated inhibition was suppressed by application of antagonists (Lee et al., 2001; Isa et al., 1998; Saito and Isa, 2003). This experimental model has been employed to study the neuronal mechanism of signal processing for execution of short latency visually guided orienting behaviors such as express saccades (Isa, 2002). Profiles of field potential responses in this have also been studied by analyzing field potentials at different depths of single electrode track in anesthetized rats (Katsuta and Isa, 2003). However, the spatio-temporal pattern of the signal propagation in 2-dimensional space is not yet clear.

Previous studies have shown that movement fields of individual neurons in dSC are large and coarsely tuned, which indicates that saccades with particular direction and amplitude are encoded by a large population of dSC neurons (McIlwain, 1975, 1982; Sparks 1986; Lee et al., 1988). Therefore it is necessary to study the activity of a population of neurons in the local circuit of the SC to clarify the role of the SC in saccade control and cognitive functions reflected in saccade performance.

In this study, the spread of activity from the sSC to the dSC was analyzed to reveal the neuronal connections in the SC slices and the signal processing through the intrinsic visuomotor pathway. We have introduced MED-system (Oka et al., 1999), in which 64-channels multi-electrode array is attached to the dish on which an SC slice is mounted, to study the spatio-temporal profile of field potentials (Fig. 2.1). The electrical stimulation might activate the passing fibers that send the signal to the neurons in remote area, so there is an argument for actual site of stimulation in this experimental model. We have confirmed our results by using the photo-stimulation system that activated only the desired population of neurons. We also combined the MED-system with whole cell recordings from single neuron to clarify the relationship between the field potentials and the intracellular potentials of individual cells in the network. Validity of this recording technique to clarify the spatio-temporal properties of spread of activity on the SC map will be shown as well as its limitation.

Materials and Methods

The experimental protocol was approved by the Animal Research Committee of the National Institute of Natural Science. All efforts were made to minimize both the suffering and number of animals used in this study.

Slice preparations

Coronal, sagittal, or oblique slices (300 μm thick) of the SC were prepared from C57BL/6, 16- to 22-day-old mice. The animals were deeply anesthetized with ether and decapitated. The brains were quickly removed and submerged in ice-cold modified Ringer solution for 4-6 min. The modified Ringer solution contained (in mM) 200 sucrose, 2.5 KCl, 1.25 NaH_2PO_4, 10 $MgSO_4$, 0.5 $CaCl_2$, 26 $NaHCO_3$, and 11 glucose and was bubbled with 95% O_2-5% CO_2 (pH 7.4). Slices were then cut with a Microslicer (DTK-2000, Dosaka EM, Japan) and incubated in standard Ringer solution at room temperature for more than 1 h before recording. The standard Ringer solution contained (in mM) 125 NaCl, 2.5 KCl, 2 $CaCl_2$, 1 $MgCl_2$, 26 $NaHCO_3$, 1.25 NaH_2PO_4, and 25 glucose and was bubbled with 95% O_2-5% CO_2 (pH 7.4).

Recordings and analysis

1. Field Potential Recording

Preparation of multielectrode array. As shown in Fig.2.1, the MED probe (MED-P5155 Panasonic; Osaka, Japan) consisted of an array of 64 planar microelectrodes, each 50 × 50 μm, arranged in an 8 × 8 pattern with a 150 μm interpolar distance. For sufficient adhesion of the slice to the probe, the surface of the MED probe was treated with 0.1%

polyethylenimine (Sigma, USA) in 25 mM borate buffer, pH 8.4, for 8 hr at room temperature. The probe surface was rinsed three times with sterile distilled water before use.

Electrophysiological recording. Slices were placed on the center of the MED probe, positioned to cover the 8 × 8 array, on an upright microscope (DM LFS, Leica, Germany) and continuously perfused with the standard Ringer solution at 33-34°C. The slices were then left for 15 min to sufficiently attach to the electrode array. A single planar microelectrode of the 64 available was selected by the 64-switch box and used for stimulation. Bipolar constant current pulses (180 μA, 0.1 ms negative pulse and 0.1 ms positive pulse) were initiated by the data acquisition software (MED64 Condutor 3.1TM, Panasonic, Japan). Evoked field potentials at the remaining 63 sites in the SC slices were recorded simultaneously with the multi-channel recording system (MED64 system, Panasonic, Japan) at a 20 kHz sampling rate. To examine the effects of antagonists, bicuculline methobromide (Bic; 10 μM), 6-cyano-7-nitroquinoxaline-2,3-dione (CNQX; 10 μM) and D-2-amino-5-phosphonovaleric acid (APV; 50 μM) (all from Sigma, USA) were bath perfused.

Current source density (CSD) analysis. A 2-dimensional CSD analysis method was employed (Shimono et al., 2002). The field potential responses were recorded with low-pass filtering at 100 Hz. The data were spatially smoothed by 3x3-weighted average kernel (0 1/8 0, 1/8 1/2 1/8, and 0 1/8 0), and the results were convolved with a 3x3

Laplacian kernel (0 1 0, 1 -4 2, and 0 1 0) to produce a discrete approximation. The medium was considered ohmic with a homogeneous conductance.

Photostimulation system. The Ultraviolet (UV) laser system (*Explorer* Laser, Spectra Physics Laser, USA) emitted UV light from an argon ion laser delivered through a 40x water immersion objective of the upright microscope (BX61WI, Olympus, Japan) and focused on the slice (Fig. 2.9*B*). The diameters of laser beam were controlled by the size of the pin-hole as between 5-150 μm. In this study, we used 5-μm diameter laser beam. The 300 μM caged glutamate (MNI-caged-L-glutamate, Tocris, USA) was applied in bath perfusion for 5-10 minutes before UV laser test. The glutamate molecule is released by the photolysis reaction as shown in figure 2.9*A*. The laser was emitted in multiple-pulse fashion; each photo-stimulation consisted of 10 pulses with 0.1 ms duration and 1 ms interval.

2. Whole-cell patch clamp recordings

Electrophysiological recording. In some experiments, whole cell patch-clamp recordings were performed under visual control of patch pipettes from the neurons in the SC slices simultaneously with the multi-channel field potential recordings. Patch pipettes were prepared from borosilicate glass capillaries and were filled with the following internal solution containing (in mM) 150 K-gluconate, 10 KCl, 0.2 EGTA, 2 $MgCl_2$, 2 Na_2ATP, 0.5 Na_3GTP, 10 HEPES and 0.1 spermine (pH 7.3). To stain the recorded neurons, biocytin (5 mg/ml; Sigma, USA) was dissolved in the internal solution. The resistance of the electrodes was 4–8 MΩ in Ringer solution. The actual membrane potentials were

corrected by the liquid junction potential of –10 mV. The osmolarity of the intrapipette solution was 280–290 mOsm/L. The whole cell recordings used a patch clamp amplifier (EPC-7, Heka, Germany) connected through a Digidata1322A analogue/digital interface card (Axon Instrument, USA). The data were acquired using a pClamp system (pClamp 8.1, Axon Instruments, USA).

Histological procedures. After whole cell recordings, slices were fixed with 4% paraformaldehyde in 0.12 M phosphate buffer (pH 7.4) for more than two days at 4°C. After fixation, biocytin-filled neurons were visualized by the ABC method. Details are described elsewhere (Isa et al., 1998).

Results

Effects of sSC stimulation on field potential of different layers

Single pulse stimulation at 180 μA in the ventral part of the sSC (SO, open square in Fig. 2.2*A*) evoked a negative field response (Fig. 2.2*B*, *C*, Cont) with short latency and short duration (latency; 3.05± 2.09 ms, duration; 82.37 ± 37.40 ms, n = 32 slices, average ± SD) in the adjacent electrode (in this case, recording electrode No. 1) just dorso-lateral to the stimulation. On the other hand, the negative field response was smaller and the latency longer at electrode No. 2, located ventrally to No. 1 in the sSC. No clear negative response was observed in the dSC (electrode Nos. 3 and 4). These results indicate that stimulation in the sSC induced excitatory synaptic potentials in the sSC, but that measurable field potentials were not generated in dSC.

In contrast, when 10 μM Bic, a $GABA_A$ receptor antagonist, was applied, the same stimulation induced much larger and longer negative responses (Fig. 2.2*B*, *C*, Bic) at electrode Nos. 1 and 2 (duration; 121.77 ± 55.95 ms, averaged from responses at recording electrodes in sSC from 32 slices). In addition, a large positive field response was observed at electrode Nos. 3 and 4 with a latency similar to the negative field response at No. 1 (Fig. 2.2*C*), and prior to the negative response. At electrode No. 3, the initial positive response started to decline at a latency of 21 ms, became negative at 64 ms, and lasted for 283 ms. The averaged duration of responses at recording electrodes in the dSC from 32 slices was 352.10 ± 132.10 ms. Such biphasic, positive-negative, field responses were observed also at electrode site No. 4, but the time course was slower than that at electrode No. 3. Thus, the negative field responses appeared to have spread gradually within dSC.

These large, long duration responses were greatly reduced by co-application of 50 μM APV, an NMDA receptor antagonist (Fig. 2.2*B*, *C*, Bic+APV). The subsequent addition of 10 μM CNQX, an AMPA/Kainate receptor antagonist, almost completely suppressed the responses (Fig. 2.2*B*, *C*, Bic+APV+CNQX). The above results were reliably observed in all 32 slices.

Spread of activity over 64-channel recording sites

The evoked responses from all 63 recording electrodes are shown for the control, Bic, and Bic+APV conditions in figure 2.3*A*, *B*, and *C*, respectively. The traces at stimulating electrodes, in the open red squares, were calculated by interpolation from the horizontally adjacent electrodes. To illustrate the spatio-temporal profile of the field potential responses, 2-dimensional, computed color images were constructed from the 63 channel data and interpolated for display (Fig. 2.3*D*, *E* and *F*). Electrical stimulation at sSC (marked with closed white squares) induced negative field potentials with short latency under control conditions. The stimulation evoked negative responses dorsal to the stimulation site. This may reflect the fact that afferent pathways to the sSC, such as the retinotectal and corticotectal fibers travel in the SO, and ascend through SGS in a ventral to dorsal direction before synapsing with dendrites of the sSC neurons in the dorsal portion of the SGS. Positive field responses were observed ventral to the stimulation, which represents the current source. The negative field potential in the sSC did not appear to have spread to the dSC. However, after application of 10 μM Bic (Fig. 2.3*E*), the same stimulus induced a large negative field response with long duration that spread widely to the dSC. The stimulation initially induced large negative responses across the dorsal portion of the sSC. This region became a strong current sink and the layers ventral

to the stimulation site became a huge source of current. Then the negative responses gradually spread within the dSC for about 60 ms after the stimulation. The activation field was expanded at around the border between the sSC and dSC, and became as wide as 1 mm in the horizontal direction in the dSC. The activation field gradually shifted ventrally in the dSC and disappeared about 300-500 ms after stimulation. These large, long lasting responses did not occur in the presence of Bic and 50 μM APV; only a short latency small response was present in the sSC (Fig. 2.3*F*).

To obtain measures of current sources and sinks of the evoked responses shown in Figure 3, 2-dimensional CSD analysis was performed (Fig. 2.4). The evoked response could be characterized as a current sink-source dipole and the current sink gradually shifted ventrally to the dSC (Fig. 2.4*D*). The current sink occupied a narrower range (Fig. 2.4*D*) than did the respective field potentials (Fig. 2.3*B*). Then, the CSD appeared to have disappeared shortly after the activation spread into the dSC. In general, CSD analyses are in good agreement with the location of synaptic inputs when the focus of activation is narrow, for instance, in the case of cerebral cortex (Mitzdorf and Singer, 1978). In the present case, however, especially after Bic application, a large excitation was induced in a wide area over the sSC and dSC. In such a case, if we take differentiation of the field potentials recorded at adjacent sites, all of which were strongly activated by excitatory input, the result does not properly reflect the activated areas activated by excitatory synaptic inputs. This appears to be a limitation of the CSD analysis in the present case. Thus, we decided not to use the CSD analysis and applied only field potential analyses in the following sections.

Relationship between the field recordings and intracellular potentials

To clarify the relationship between the field responses and intracellular potentials, we analyzed the electrically evoked responses in individual neurons from sSC (in the SGS and the SO) and from dSC (in the SGI) by whole-cell patch-clamp recording simultaneously with the field potential recordings. The slices were stimulated by the planar electrodes located at the dorsal portion of the SGS. Neurons at the edges of the planar electrodes, < 50 μm, were randomly selected for recording and the intracellular potentials were compared with the field recordings. Under control conditions (Fig. 2.5*A*), sSC stimulation elicited monosynaptic EPSPs, as judged from their short, fixed latencies (~3 ms), in both of the 2 SGS cells recorded in the present study. The field potentials close to this cell exhibited negative potentials with time courses similar to those of the intracellular EPSPs. SGS stimulation also induced monosynaptic EPSPs in all the 11 recorded SO neurons. Negative field responses were also induced in the SO, but usually the amplitude was smaller than that recorded in the SGS. Monosynaptic EPSPs were induced only in a few SGI neurons (2/16cells); in most cases SGS stimulation induced no responses in SGI neurons (14/16 cells). As described above (Fig. 2.2), SGS stimulation induced no field response in the SGI, or only a small, short latency, positive component, which was thought to represent the reversal of the negative response that originated in the SGS. After application of 10 μM Bic, the EPSPs were enhanced and bursting spike responses were induced both in sSC and dSC neurons (Fig. 2.5*B*). The duration of depolarizing responses in the SGS and SO neurons roughly corresponded to that of field potential responses recorded at adjacent electrodes. On the other hand, the duration of depolarizing responses in SGI neurons varied considerably from cell to cell. Some SGI

neurons showed transient bursts and 300 ms depolarizing responses (Fig. 2.5*B*, 3). Whereas, other SGI neurons exhibited long lasting depolarizations (longer than 1s) that outlasted the field response (Fig. 2.5*B*, 4). It should be pointed out that the latencies of the EPSPs in the SGI neurons were distributed from 2 – 17 ms (n = 16). Thus, excitation of the SGI neurons had already started, while the field potential adjacent to the intracellularly recorded cell was still in the positive phase. As shown in figure 2.5*B,* 4, onset of the EPSPs appeared to correspond to the highest depolarizing point of the field potential. Thus, in subsequent analyses of SGI neurons, we measured the duration of the negative field responses from the start of the decline of the depolarizing phase. In figure 2.6 we compared the duration of depolarizing responses of the intracellular potential with that of the negative field responses. The duration of both potentials were similar for responses in the SGS (n=2) and SO (n=11), while they varied considerably for those in the SGI (n=16). These various durations of the responses from the SGI neurons might correspond to their higher variation in morphological cell types. Actually, morphology of SGI neurons was more heterogeneous than SGS/SO neurons, however no clear relationship could be detected between the cell morphology and variation of responses. The result indicated that the SGI neurons consisted of a heterogeneous population and the field responses represent the average of synaptic potentials in the population.

Spread of activity in the parasagittal plane

The above results were obtained in coronal slices. Next, we examined the spread of excitation in parasagittal slices of the SC and compared the effects of stimulating rostral and caudal sites in the sSC in the presence of 10 μM Bic (Fig. 2.7*A*). When the rostral part of SGS was stimulated (Fig. 2.7*B*), the activation spread not only ventrally,

but also caudally to the stimulation site, eventually covering the entire rostral-caudal range of the multi-electrode array. When the stimulation was applied to a more caudal portion of the SGS (Fig. 2.7*C*), the excitation spread ventrally and caudally, activating the extent of the SC circuit caudal to the stimulation. However, the activity did not appear to spread as far in the rostral direction. The parasagittal slices were obtained from both medial and lateral SC, however there was no difference between them. Thus, when the SGS was stimulated in parasagittal slices, the activity spread asymmetrically.

Oblique slices

We interpreted the asymmetric spread of activity in the rostral-to-caudal direction in the parasagittal slice to be due to stimulation of the optic tract, which passed through the optic layer from the rostro-lateral to the caudo-medial direction (Fig. 2.8*B*). To examine this further and to establish a preparation that avoids activating passing axons of the optic tract, we tested oblique slice preparations of SC cut in the rostro-medial to caudo-lateral plane, perpendicular to the direction of the optic fiber axons. When a stimulation pulse was applied to the optic layer in the rostral portion of the slice (Fig. 2.8*A*), no rostro-caudal spread of the activation was observed in the presence of Bic in all 12 slices tested, as exemplified in figure 2.8*C*. The area of activation spread just from a dorsal to ventral direction. This observation supported the assumption that in the parasagittal slices, stimulation of the optic layer at the rostral portion of the SC induced activity that spread in a rostral to caudal direction, along the trajectory of the optic fibers.

Spread of activity evoked by photostimulation system

To confirm our findings, we have compared the results obtained by two stimulation systems in the same slice, the electrical stimulation from MED64 system and

the photo-stimulation system. We stimulated by using both system at the same location as shown in blue squares and red circles in figure 2.10*A* and *B*, respectively. 10 μM Bic were applied to the bath perfusion in both conditions. The UV laser was applied to specific areas, 5 μm in diameter, on slices to release free glutamate from a chemical bond with a large molecule called "caged glutamate". Figure 2.10*C* demonstrated the field responses (red traces) induced by the uncaged glutamate that activated only the neuron not the fiber of passage compared to the response induced by the electrical stimulation (blue traces). Although the electrical evoked response showed the faster and sharp negative potential than chemically evoked responses due to the slower kinetic of chemical stimulation, the patterns of signal spread of both stimulation systems were similar. The recording electrode close to the stimulated location showed negative-phase response, then the signal propagated ventrally to the dSC where activity was spread to wide area. Therefore, we might safely avoid stimulation of long-range passing fibers in case of the electrical stimulation experiments.

Discussion

Field potential recordings in SC slices

A previous study of anesthetized rats from our laboratory (Katsuta and Isa, 2003) showed that electrical stimulation of the optic fibers at 2 mA, which activated both Y and W-fibers, induced negative field responses in the most dorsal part of the sSC, while a reversed positive potential was observed in the ventral part of the sSC and in the dSC. Such a current sink and source relationship might be derived from neurons with cell bodies in the ventral part of the sSC or in the dSC and dendritic arborizations in the dorsal part of the sSC that receive input from the optic tract. These neurons include narrow-field and wide-field vertical cells (Langer and Lund, 1974; Isa and Saito, 2001). In normal controls, no clear negative responses were observed in the dSC. However, when Bic was injected into the dSC, a large, long lasting negative response was evoked in the dSC that followed a positive potential. A similar pattern of activation was observed in anesthetized macaque monkeys (Nikitin and Isa, 2004). In the present study, field responses with similar profiles were detected by multichannel field potential recordings in slice preparations of the SC. This methodology enabled us to better understand how the effects of a single stimulus pulse in the sSC spreads within the dSC. We demonstrated, for example, that the activation zone of such stimulation spreads more than 1 mm in the horizontal direction and its center gradually shifts from the dorsal to ventral portion of the dSC. Thus, spatio-temporal patterns of activity spread could be analyzed in a 2-dimensional plane, which is difficult in whole cell recordings from 1 or 2 cells. To understand the actual site of synaptic activation, we performed a 2-dimensional CSD analysis; however, although the CSD analysis could narrow the focus of activation, it did

not appear to correctly reflect the distribution of activity in situations where the activity spread so widely and homogeneously throughout the network. Therefore, we decided to rely on analyses of field potential profiles. The limitation is that the field potential shows the relative amount of excitation among various locations of the circuits along a particular direction determined by the dendritic geometry, and not the absolute intracellular membrane potentials of neurons in individual locations. For instance, in the present study, after application of Bic, SGS stimulation induced large negative responses in the sSC, which reflected the EPSPs in the neurons therein; however, it simultaneously induced large positive responses in the dSC. The positive potential did not indicate that the dSC neurons were concurrently hyperpolarized, but simply indicated that the dSC became the current source of activities in the sSC. In support of this argument, the simultaneous whole cell recordings indicated that some dSC neurons had already received excitatory synaptic inputs and were depolarized when the field potential adjacent to the intracellularly recorded cell was still in the positive phase. Thus, the field potential analysis did not always clearly illustrate the onset of excitation in dSC neurons, which seems to be the most important limitation of this approach. However, as shown in figure 2.5*B*, the peaks of the positive potentials, that is, the start of the decline of the positive phase, closely corresponded to the onsets of EPSPs in the dSC neurons. This information might be useful for further improvement of this technique. Except for this limitation, the multichannel field potential recording system should be a powerful tool for studying spatio-temporal profiles of the spread of activity in the local circuit of the SC. Since such a current sink-source relationship occurred in the dorso-ventral direction (dorsal-negative vs ventral-positive) but did not appear to occur in the horizontal

direction both in the sSC and dSC or in the adjacent region of the dSC. Thus, the distribution of field potential is asymmetric. Moreover, a large negative field response in the dSC never produced a positive field response in the sSC, which might reflect the dendritic geometry of dSC neurons such as wide field vertical cells as described above. Our findings in electrical stimulation protocol were confirmed by laser uncaging of a caged glutamate compound that selectively activates the cell bodies and dendrites at the sites of stimulation and avoids activation of passing fibers (Lee et al. 2007).

Complication of electrical stimulation

It was surprising that when the sSC (actually, SO) was stimulated in parasagittal slices, the activity spread extensively in the ventral and caudal directions, but not in the rostral direction (Fig. 2.7). This asymmetry was not evident in coronal slices. We interpreted this rostrocaudal asymmetry to the activation of optic fibers. The optic fibers enter the SC at its rostrolateral part and travel through the SO a rostro-lateral to caudo-medial trajectory. Therefore, in sagittal slices, electrical stimulation of the sSC activated the optic tract, and the signal spread from the rostral to caudal direction. This was further demonstrated in the experiments shown in figure 2.8; in the slices cut perpendicularly to the course of the optic tract, the sSC stimulation induced a dorsal-to-ventral spread of activity in a narrow range in the horizontal direction. Such spread of activation in the rostro-caudal direction also appeared to occur *in vivo* during visually guided saccades. In previous studies, when the rostral portion of the SC, which encodes small amplitude saccades, was stimulated, the evoked saccades tended to be larger than the eccentricity of the response field of the cells at the stimulation sites (Van Opstal et al., 1990). Such observations may be explained by the rostral to caudal spread of activation along the

optic tract, which results in a more caudal location of the center of activation than the site of stimulation.

Functional implication

The results of the present study has clearly shown that the effect of single pulse stimulation of the sSC does not excite the neurons in the dSC by itself, however, the same stimulus induces a large and long lasting excitation of a large population of dSC neurons when the $GABA_A$ receptor-mediated inhibition was reduced. Such direct signal transmission from the sSC to the dSC is supposed to occur in case of express saccades, extremely short latency orienting responses (Isa, 2002). One might suppose that the time course of signal transmission from the sSC to dSC as shown in the present results might look too slow for generation of express saccades, however it should be kept in mind that the onset of the negativity in the dSC does not indicate the onset of excitation in dSC. It has been shown that saccade-related burst neurons in the dSC are tonically inhibited by the substantia nigra pars reticulata during fixation (Hikosaka and Wurtz, 1983). In addition, fixation neurons in the rostral pole of the SC also tonically inhibit saccade-related burst neurons via local GABAergic interneurons (Munoz and Wurtz, 1993a, 1993b; Meredith and Ramoa, 1998). It has been reported that fixation neurons decrease firing prior to saccade onset (Dorris et al., 1997). Moreover, their decrease in firing is more predominant in case of express saccades than in case of saccades with regular latencies. Thus, reduction of tonic GABAergic inhibition actually occurs in case of express saccades. Moreover, our recent study on recordings from SGI GABAergic neurons using GAD67 GFP knock-in mice showed that many of these inhibitory interneurons exhibit tonic firing in slices (Sooksawate T, Isa K, Yanagawa Y, Isa T,

unpublished observation). Therefore, our current experimental manipulation in slices mimics the condition for express saccade generation in vivo.

Striking finding of the present study is that neurons extending in a large area of the dSC can be synchronously activated. The area of the negative field potential spanned as long as 1 mm in the horizontal direction, that is, more than half area of the SC, which supports the population coding in the dSC. In addition, the center of gravity of the excitation moved in the dorsal-to-ventral direction in coronal slices, where contamination of passing fiber stimulation is negligible. It has been proposed that activated neuronal population might shift from the caudal to rostral direction during saccades (Munoz et al., 1991; Munoz and Wurtz, 1995). However, no sign of such "moving hill" phenomenon was observed in this study. Thus we could not obtain evidence which positively suggests that "moving hill" mechanism is implemented in the local circuit mechanism of the SC.

Our recent report showed that NMDA receptors in the sSC play a critical role in burst generation in the dSC (Kaneda et al. 2008). The present study did not directly examine this issue, however the results clearly showed that the area of negative field potential is considerably expanded at the border between the sSC and dSC. Further studies are necessary to elucidate the neural mechanism critical for triggering the burst generation in the SC local circuit.

Figure legends

Figure 2.1. Introduction of the recording system. ***A,*** The Multielectrode Dish (MED). ***B,*** A higher magnification view of an 8×8 array of 64 planar microelectrodes with aninterpolar distance of 150 μm located at the bottom of the dish. The size of eachelectrode is 50×50 μm. ***C,*** The microelectrode structure. The surface of each electrode iscoated with platinum black, resulting in a dramatically low impedance (7-10 KΩ). ***D,*** Fresh coronal slice of the SC overlying a multi-electrode array. The *stratum griseumsuperficiale* (SGS) and the *stratum opticum* (SO) are in the superficial layer (sSC). The*stratum griseum intermediale* (SGI), *stratum album intermediale* (SAI), *stratumgriseum profundum* (SGP), and *stratum album profundum* (SAP) are in the deeper layer (dSC).

Figure 2.2. The field responses evoked by stimulation in the sSC. ***A,*** The position ofmicroelectrodes on a slice. The boundary between sSC and dSC is indicated by a white line. The electrode outlined in white was the stimulating electrode and the remaining 63 electrodes were recording electrodes. The responses from electrodes 1-4 are shown in *B*. ***B,*** Field potentials from representative electrodes 1-4 elicited by a biphasic pulse (positive 0.1 ms and negative 0.1 ms, 180 μA) to the stimulating electrode under fourconditions, control (Cont), 10 μM bicuculline (Bic), 10 μM Bic and 50 μM APV (Bic+APV), and 10 μA Bic, 50 μM APV and 10 μM CNQX (Bic+APV+CNQX). ***C,*** The same records shown within the dotted lines in *(B),* but in a faster time sweep and focused on the events shortly after the electrical stimulation.

Figure 2.3. The spatial distribution of the field responses. ***A, B, C,*** The 64-channel field potentials (the same results as those shown in Fig. 2*B*) in the Control, Bic**,** and Bic+APV conditions, respectively. Gray curved lines indicate the boundary between sSC and dSC and the ventral border of the dSC. Gray curved dotted lines indicate the boundaries between the SGS/SO and SGI/SAI layers. ***D, E, F,*** Computed color images of field potentials from ***A, B, C,*** respectively, demonstrate the spatial distribution of responses at each time point. As indicated in the color bar, negative potentials are in red

and positive ones in blue. White lines indicate the dorsal boundary of the SC, boundary between the sSC and dSC and ventral border of the dSC. The locations of stimulating electrodes are shown by the white squares.

Figure 2.4. The current source density (CSD) analysis. ***A, B,*** Results of CSD analyses are shown in red traces, while the raw field potential data are in black traces under control (*A*) and Bic (*B*) conditions. ***C, D,*** Computed color images of the CSD results from (*A*) and (*B*), respectively. As shown on the color bar, sinks are shown in red and sources in blue.

Figure 2.5. Representative response pairs showing the comparisons of durations in whole cell and field recording. The duration of EPSPs (Intra) recorded by patch-clamp were compared with the field potentials (Field) recorded from the electrode nearest the recorded cells in the control (***A***) and 10 μM Bic conditions (***B***). The stimulating electrodes were located in the SGS in all slices. These four sample pairs were selected from various locations, ***1,*** SGS, ***2,*** SO and ***3, 4,*** SGI. The numbers in parentheses indicate the locations of each neuron as shown in Figure 6*A*.

Figure 2.6. Comparisons of response durations in whole cell and field recordings. ***A,*** A schematic illustration showing the location of recorded cells on the slice (29 cells). ***B,*** Comparison of response durations of the EPSPs (opened circle) and the negative phase of the field responses (closed circle).

Figure 2.7. **The spread of activity in parasagittal sections.** ***A,*** The position of multi-electrodes on a slice. The boundary between layers (the sSC and the dSC) is indicated by a white line. The white squares (1) and (2) show the stimulating electrodes in (***B***) and (***C***), respectively. ***B, C,*** Computed color images of field potentials evoked from a biphasic pulse to the Stim 1 and Stim 2 electrodes and recorded from the remaining 63 electrodes in the presence of Bic. Representative images from n=16 slices.

Figure 2.8. **The spread of activity in oblique sections (perpendicular to OT)**. The slice was cut in the oblique direction to avoid an effect of optic fiber stimulation. ***A,*** Position of electrode on the slice. ***B,*** A schematic illustration of the cutting direction. ***C,*** The computed color images of field potentials evoked from a biphasic pulse to the electrodes marked with a white square. Representative images from n=12 slices.

Figure 2.9 The uncaging-photostimulation system. ***A,*** The photolysis reaction that releases free L-glutamate for local activation of the neurons in specific area. ***B,*** UV light from the laser was delivered through a 4x objective lens, and focused on the slice. 4-Methoxy-7-nitroindolinyl-caged L-glutamate (MNI-caged glutamate) dissolved in the bath solution was photolyzed over an area of laser beam in the slice. The Spectra-Physics Explorer systems are an all solid-state, Q-switched lasers that produce ultraviolet pulses at adjustable repetition rates up to 5 kHz.

Figure 2.10. **The field potential response evoked by the photostmulation system**. ***A***,***B,*** The position of multi-electrodes on a slice. The boundary between layers (the sSC and the dSC) is indicated by a white line. The blue squares in (A) and red circle in (B) show the electrical stimulating electrode and photolysis laser beam location, respectively. ***C,*** The field potential responses evoked by the electrical stimulation (blue trace) and the uncaging-photostimulation (red trace). 10 μM Bic was applied to both stimulus conditions. ***D,*** Computed color images of field potentials induced by both systems, compared in the same temporal scale. White lines indicate the boundary of slice and borders between layers.

Figure 2.1

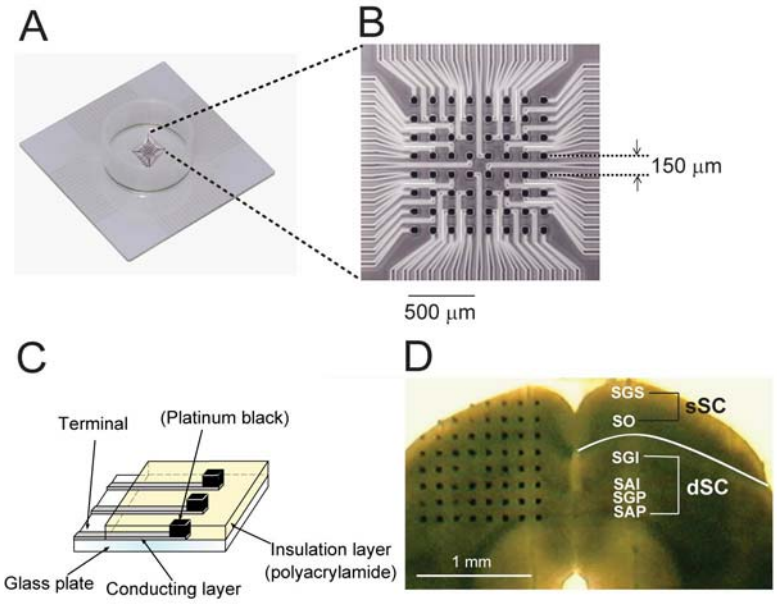
A
B
150 μm
500 μm
C
Terminal
(Platinum black)
Insulation layer
(polyacrylamide)
Glass plate
Conducting layer
D
SGS
SO
sSC
SGI
SAI
SGP
SAP
dSC
1 mm

Figure 2.2

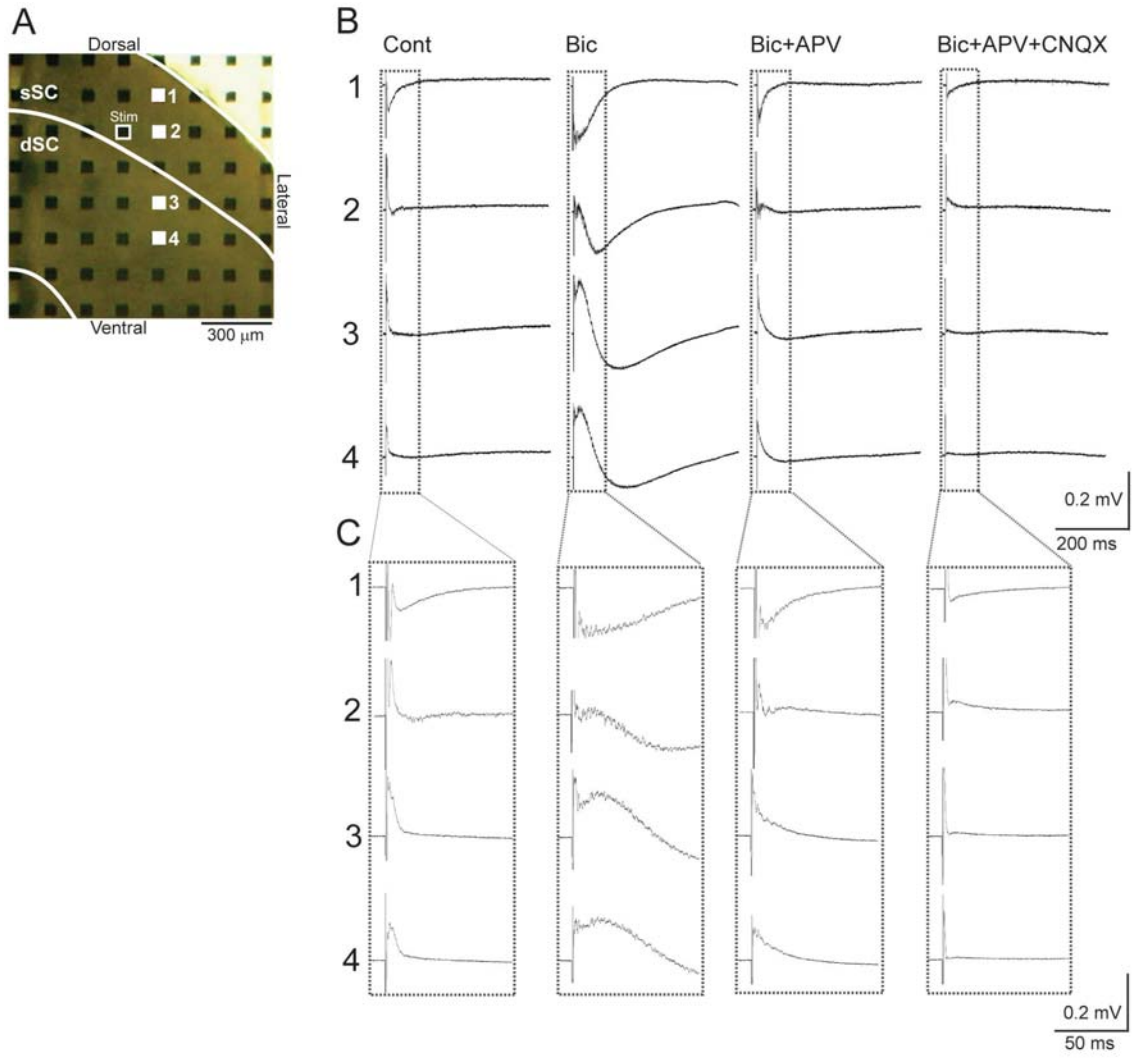
A
Dorsal
sSC
dSC
Stim
1
2
3
4
Lateral
Ventral
300 μm
B
Cont
Bic
Bic+APV
Bic+APV+CNQX
1
2
3
4
0.2 mV
200 ms
C
1
2
3
4
0.2 mV
50 ms

Figure 2.3

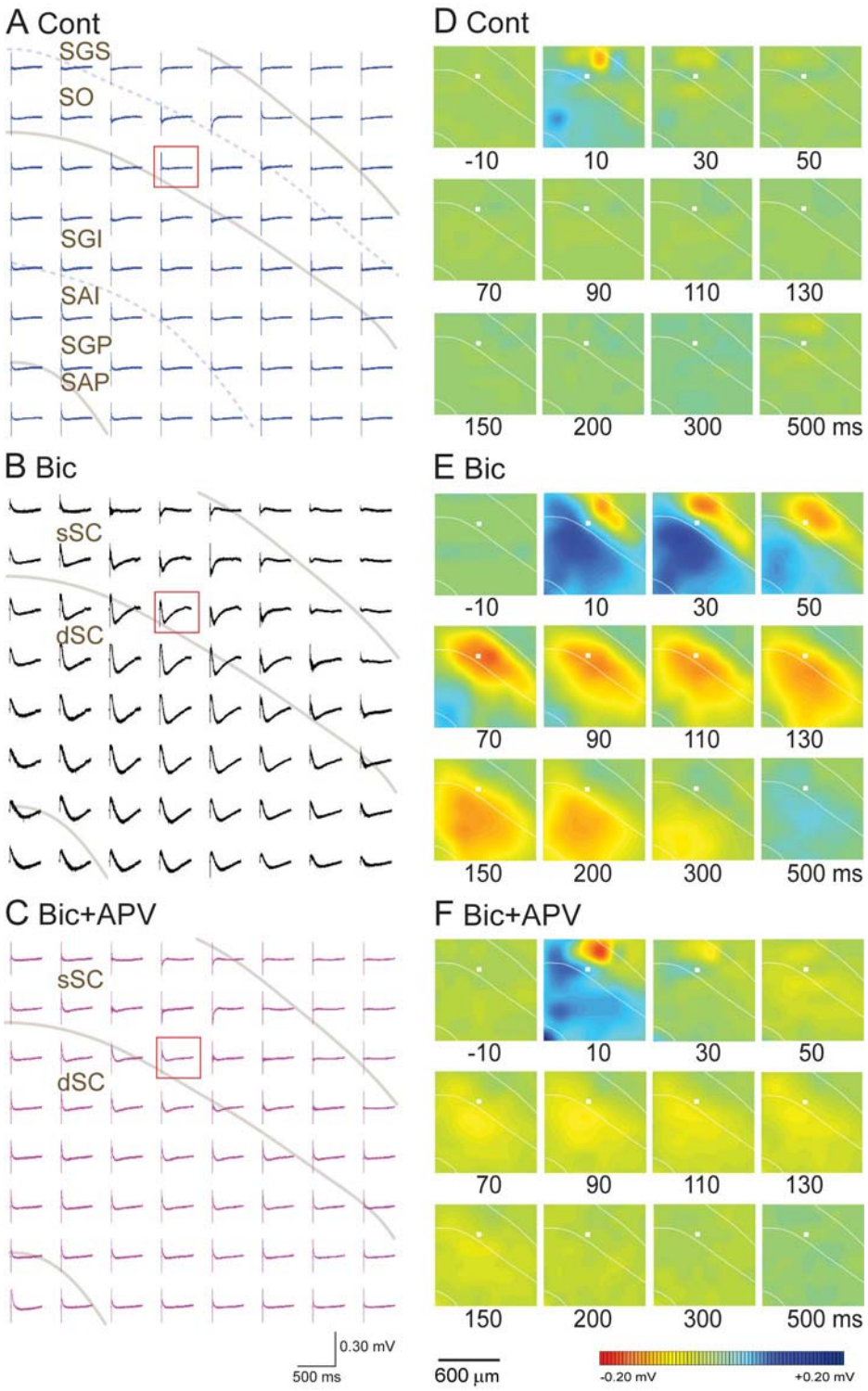
A Cont
SGS
SO
SGI
SAI
SGP
SAP
B Bic
sSC
dSC
C Bic+APV
sSC
dSC
0.30 mV
500 ms
D Cont
-10
10
30
50
70
90
110
130
150
200
300
500 ms
E Bic
-10
10
30
50
70
90
110
130
150
200
300
500 ms
F Bic+APV
-10
10
30
50
70
90
110
130
150
200
300
500 ms
600 µm
-0.20 mV
+0.20 mV

Figure 2.4

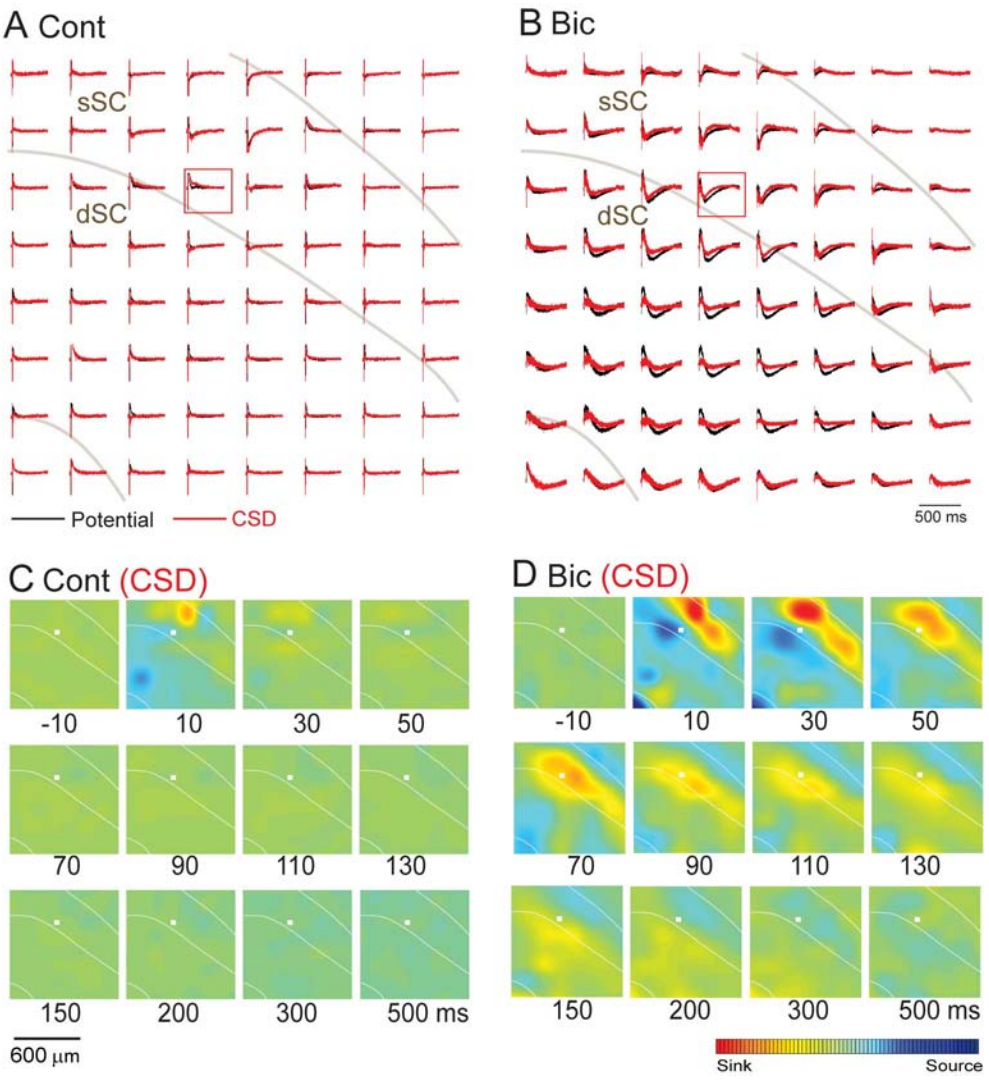
A Cont
sSC
dSC
Potential
CSD
B Bic
sSC
dSC
500 ms
C Cont (CSD)
-10
10
30
50
70
90
110
130
150
200
300
500 ms
600 μm
D Bic (CSD)
-10
10
30
50
70
90
110
130
150
200
300
500 ms
Sink
Source

Figure 2.5

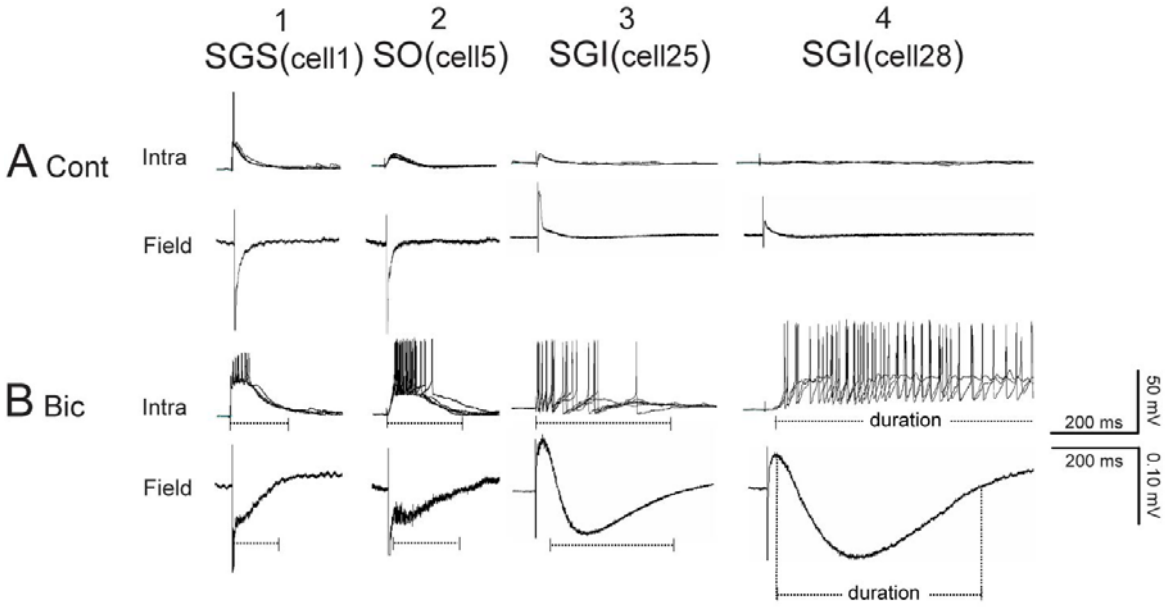
1
SGS(cell1)
2
SO(cell5)
3
SGI(cell25)
4
SGI(cell28)
A Cont
Intra
Field
B Bic
Intra
Field
duration
duration
200 ms
50 mV
200 ms
0.10 mV

Figure 2.6

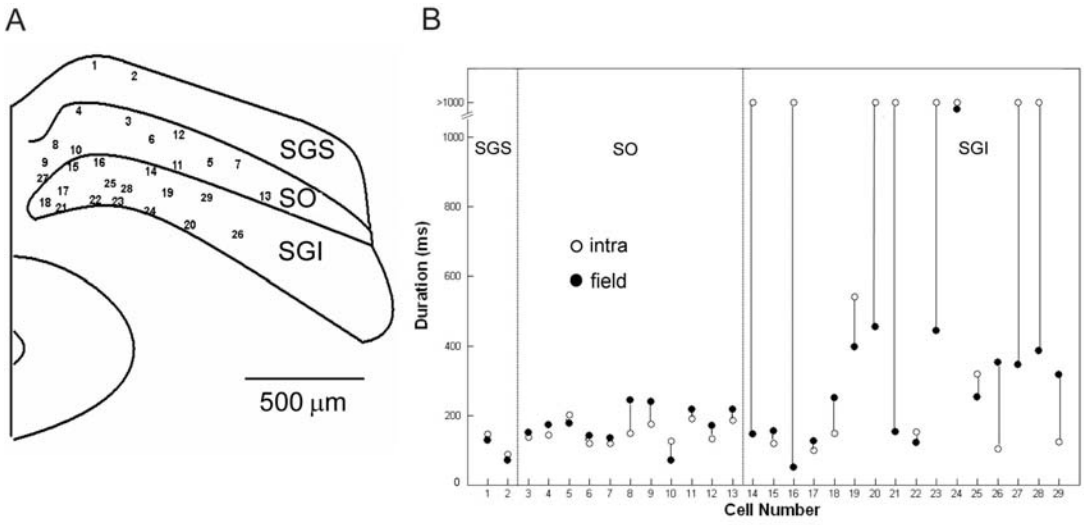
A
B
SGS
SO
SGI
500 μm
SGS
SO
SGI
intra
field
Duration (ms)
Cell Number

Figure 2.7

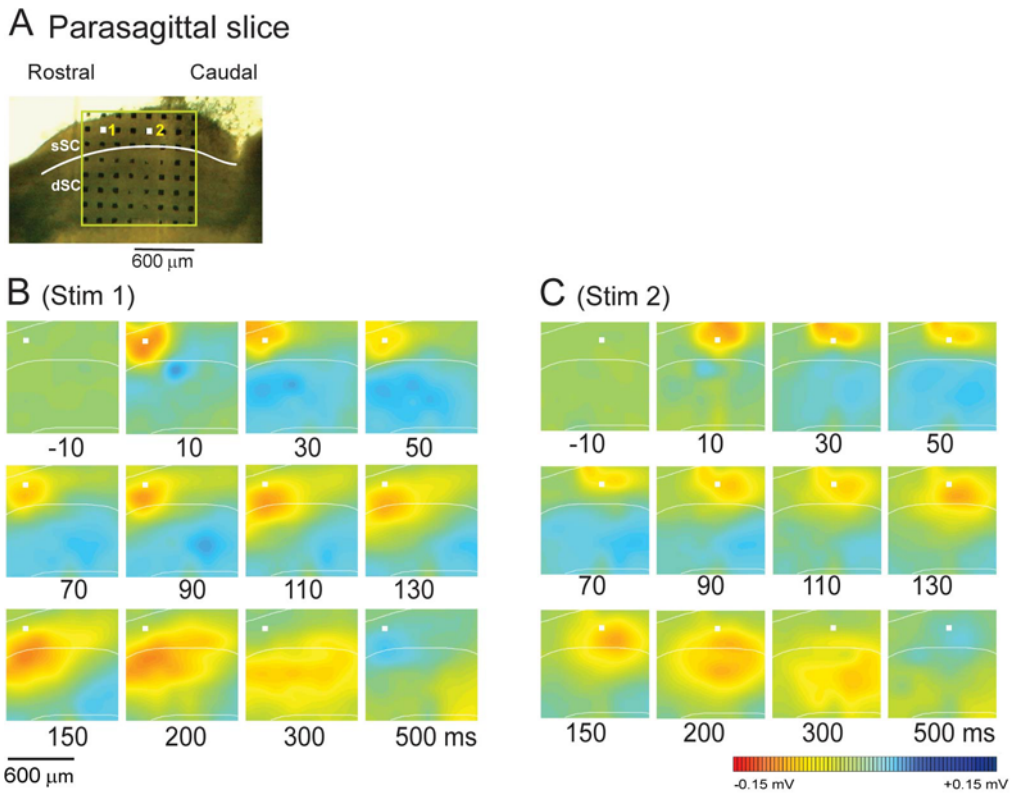
A Parasagittal slice
Rostral
Caudal
sSC
dSC
1
2
600 µm
B (Stim 1)
-10
10
30
50
70
90
110
130
150
200
300
500 ms
600 µm
C (Stim 2)
-10
10
30
50
70
90
110
130
150
200
300
500 ms
-0.15 mV
+0.15 mV

Figure 2.8

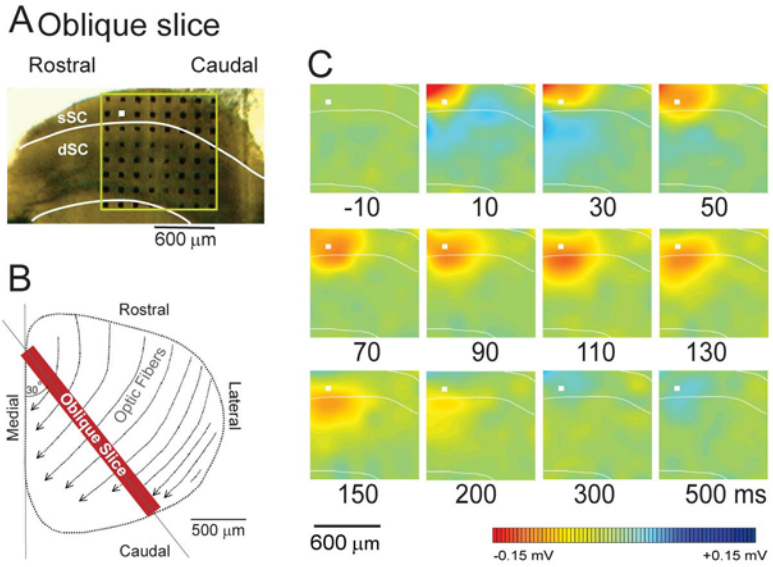
A Oblique slice
Rostral
Caudal
sSC
dSC
600 µm
B
Rostral
Medial
Lateral
Caudal
30°
Oblique Slice
Optic Fibers
500 µm
C
-10
10
30
50
70
90
110
130
150
200
300
500 ms
600 µm
-0.15 mV
+0.15 mV

Figure 2.9

A

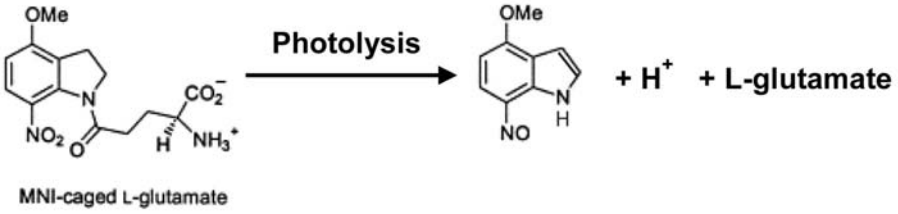
OMe
Photolysis
OMe
+ H+
+ L-glutamate
NO2
CO2−
NH3+
NO
H
MNI-caged L-glutamate

B

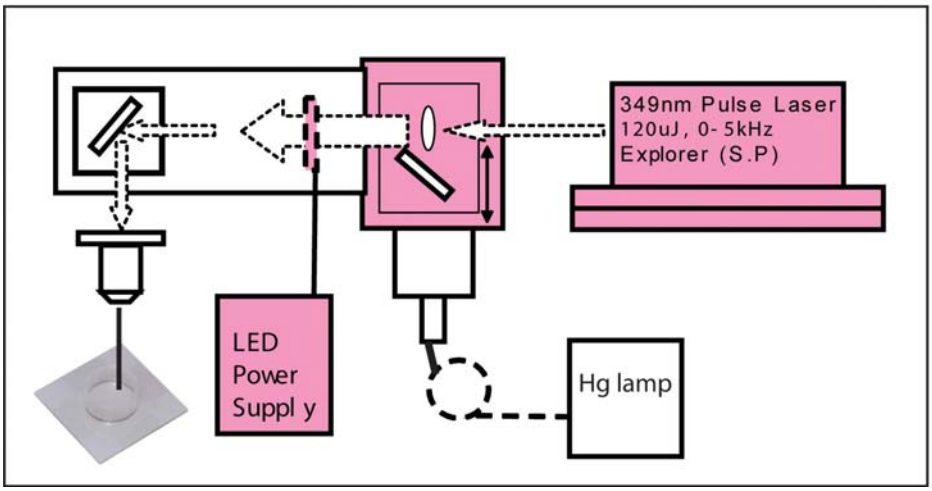
349nm Pulse Laser
120uJ, 0-5kHz
Explorer (S.P)
LED
Power
Suppl y
Hg lamp

Figure 2.10

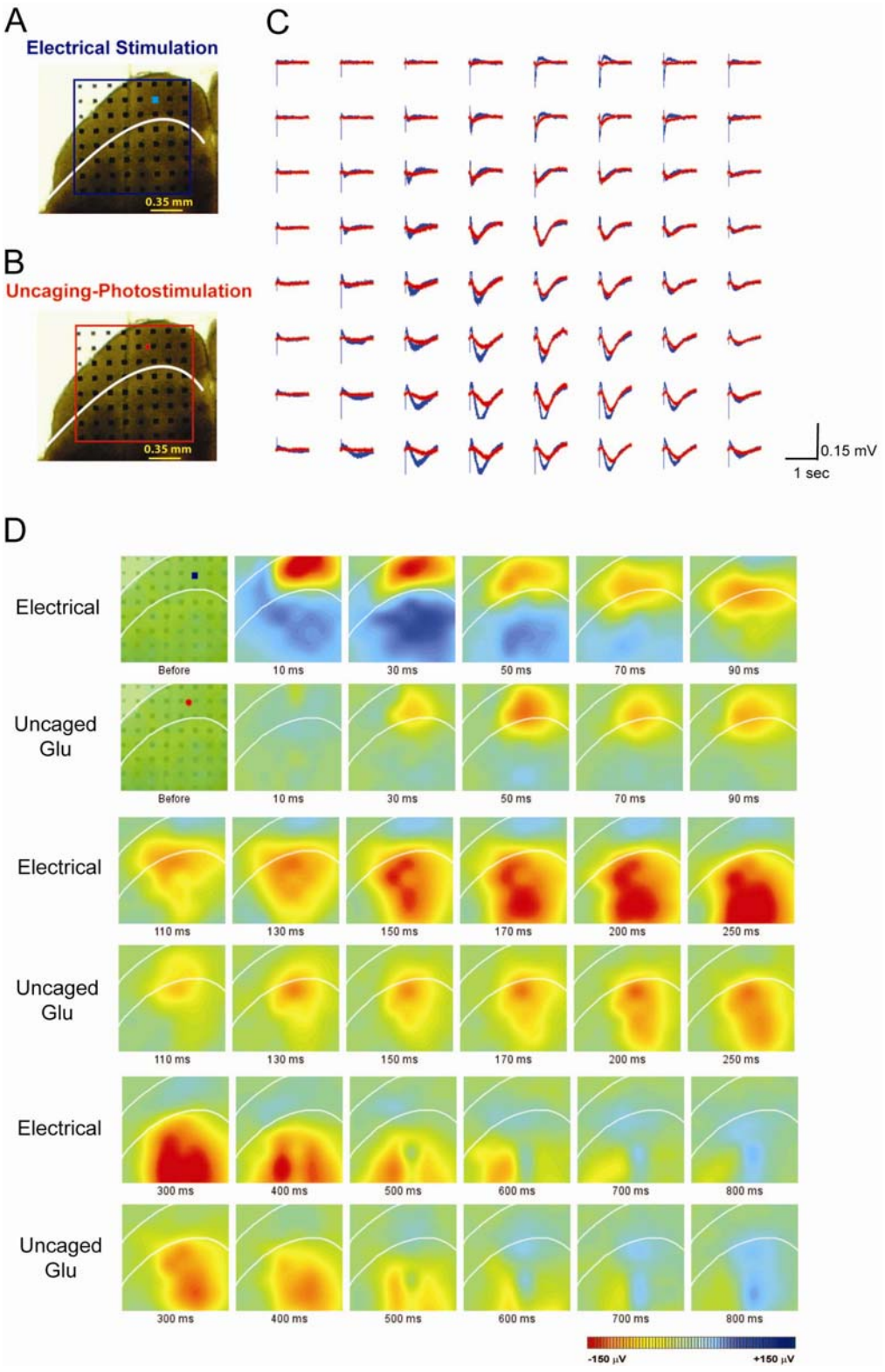
A
Electrical Stimulation
0.35 mm
B
Uncaging-Photostimulation
0.35 mm
C
0.15 mV
1 sec
D
Electrical
Uncaged Glu
Before
10 ms
30 ms
50 ms
70 ms
90 ms
110 ms
130 ms
150 ms
170 ms
200 ms
250 ms
300 ms
400 ms
500 ms
600 ms
700 ms
800 ms
-150 µV
+150 µV

Part III

Generation of synchronous burst activity in the intermediate layer

Introduction

SC neurons receive a variety of sensory, motor and cognitive information and send motor commands to brainstem gaze center. The convergence of visual input and motor preparation in the dSC suggests its functional role in the initiation of orienting behaviors such as saccadic eye movement. It is established that the activity in the dSC neurons critically affect the direction and timing of saccade (Dorris et al., 1997).

In **Part II**, we have described large populations of dSC neurons involving in the burst activity with nonlinear amplification from such a single pulse sSC stimulation in Bic application. However, we could not answer weather the signal can propagate from the dSC to the sSC or not. In this part, we used the uncaging glutamate photostimulation system to activate the neurons in different layers from SGS to SGI and compared the evoked bursts.

In previous studies, Saito and Isa (2003, 2004, 2005) have reported that when the rat SC slice was incubated in the low concentration of Magnesium (Mg^{2+}) Ringer solution and 10 μM Bic, most of the neurons in that slice exhibited spontaneous depolarization and burst firing. These spontaneous activities were proposed to share common mechanisms in presaccadic burst activity in SGI neurons. We applied this method to study the properties of the spontaneous activity in order to identify the original location of synchronous burst and examine the synchronicity of the spontaneous activity recorded by the field and whole cell recording system. In the previous study, we performed simultaneous recordings from a pair of SC neurons and proposed that the

spontaneous synchronous burst was spread as wide as 1 mm horizontally in the dSC (Saito and Isa, 2004) and it started from the the wide field vertical (WFV) cell, a specific cell group found in the ventral portion of the sSC and upper portion of SGIa layers (Saito and Isa, 2005). However, where the synchronous burst activity was generated and spread inside the SC is still unclear and should be examined using the multi-channel recording system. Although, the hyperpolarization activated current (I_h) can be found in other cell types, expression of large amplitude I_h is the well-characterized property of WFV. Therefore, to test the hypothesis that the WFV cells is the origin of the synchronous burst, we investigated contribution of I_h and WFV by application of its blocker in the spontaneous activity conditions.

In the present work, we have ruled out the possibility that the signal spread from the dSC to the sSC and showed the evidences that supported the hypothesis that the origin of burst generation is WFV cell.

Materials and Methods

This section has been described in **Part II**.

To performed the spontaneous activity recording, we used the modified Ringer solution containing 125 NaCl, 2.5 KCl, 2 $CaCl_2$, 0.1 $MgCl_2$, 26 $NaHCO_3$, 1.25 NaH_2PO_4, and 25 glucose and was bubbled with 95% O_2-5% CO_2 (in mM) with 10 μM Bic (pH 7.4).
The I_h blocker, ZD7288, was purchased from Sigma, USA.

Results

3.1 Comparison of stimulation at different layers; The dSC stimulation evoke smaller activity than the sSC

In **Part II**, the stimulation was applied only in the sSC, and it evoked short latency responses in both the sSC and dSC when 10 μM Bic was applied. In this part, the stimulations applied to various layers were examined to compare the field potential responses evoked from different locations. The photostimulation system was employed to stimulate neurons within a circle of 5 μm in diameters, which is the size of the laser beam. The field potential responses evoked by stimulation at four different locations ranging from SGS to SGIb in the presence of 10 μM Bic are shown in figure 3.1*B*. As shown the first column, stimulation in the SGS elicited strong depolarizing activity in the sSC, particularly in the dorsal part of SGS. Then, the evoked signal spread ventrally to the dSC in about 60 ms after stimulation. Interestingly, the activated area was expanded horizontally at the ventral portion of the SGS (see the 4th record from the top). The next column shows the response of SO stimulation that spread to the dSC with horizontal expansion. In the third column (Fig 3.1*B*-*3*), the border area between SO and SGIa, was stimulated. The evoked response showed considerable horizontal spread from the beginning, but the evoked response stayed around the stimulating point for about 100 ms, and did not spread either ventrally of dorsally. The response of SGI stimulation was demonstrated in the rightmost column. As the SGIa stimulation, the evoked response did not spread to the deeper portion or back spread to the dSC. This activity was restricted in its layer; however, it showed a slight shift of the center to lateral side. Now spread of activity was observed from the dSC to sSC. Basically, similar effect was observed by the

electrical stimulation of the same locations (data not shown). All these results indicate that only the sSC stimulation could evoke large and long lasting excitatory responses that spread over layer.

3.2 *Spontaneous burst was generated in the sSC and propagated to the dSC*

In a previous series of studies, the spontaneous depolarization and firing occurred in almost all the neurons when the slice was submerged in the low Mg^{2+} and Bic (Saito and Isa, 2003, 2004, 2005). To study where the spontaneous bursts are generated and how they are spread in the local circuits of the SC, we applied with our multielectrode recording system to study the spontaneous bursts. In our experiment, the spontaneous synchronous activities were observed as the large negative field responses, when the coronal mouse slice was exposed to the Ringer's solution containing low Mg^{2+} (0.1 mM) and 10 μM Bic. The samples of the spontaneous activities are shown in figure 3.2*B*. The activity recorded in all the 64 channels exhibited the similar pattern to the burst that evoked by electrical stimulation in the **Part II**, beginning with the short duration negative potential which appeared in the sSC, and the positive potential in the dSC. Then, the response in the sSC changed to a small positive response, while a long and large negative potential was induced in the dSC. As we have discussed in **Part II**, the positive potential in the dSC is supposed to represent the current source to the current sink in the sSC. It does not indicate the hyperpolarized activity.

The activity recorded by the electrode in the sSC indicated with the blue square in figure 3.2*A* is shown in figure 3.2*C* and *D*. Spontaneous burst firings were observed. Their frequencies varied from slice to slice. Various characteristics of bursts were recorded, from single bursts to complex bursts. However, in all the cases, the propagation

pattern of the synchronous activities was consistent; they propagated from the sSC to the dSC in all the tested slices (n = 21 slices). The colored images showing the spatio-temporal distribution of field potentials computed for a representative spontaneous burst (shown in Fig. 3.2*D*), between the duration indicated by the black bar above the potential trace, are shown in figure 3.2*E*. As shown in the figure, the synchronous activity was originated in the sSC and then shifted from the lateral to medial part within the sSC. Then, it propagated to the dSC where the marked amplification of the response happened, as is indicated by the large red area shown for 200-400 ms following the stimulus. The location of the largest negative potential at any given time in figure 3.2E was marked as a small square in figure 3.2*F*, and the line was drawn between these points to indicate the pathway of spread of this spontaneous burst. As shown in the figure, the center of the activity emerged first in the sSC and then moved into the dSC, which is the similar course of the activity induced by the electrical or chemical stimulation of the sSC (see **Part II**).

3.3 I_h current blocker eliminated the spontaneous activity

Whole-cell patch-clamp recordings were performed simultaneously with the field potential recording to investigate the timing relationship between the field and intracellular spontaneous activity. The WFV cells in SO layer closed to planar electrode, less than 50 μm, were selected by visual guide (Fig. 3.3*A*). All WFV cells that exhibited the spontaneous burst showed the synchronous timing of burst firing with the burst in field recording (Fig. 3.3*C*).

The Ih blocker, 50 μM ZD7288, was applied by bath application. The effect of the blocker was examined 15 minutes after application to ensure the penetration of the drug.

Application of ZD7288 eliminated all the spontaneous bursting responses in both field and current clamp recording (Fig. 3.3*D*) in all the tested slices (n = 11 slices).

Discussions

The burst initiation in the SC is critical for controlling motor command of orienting behaviors. In present works, we used the extracellular solution containing low Mg^{2+} and 10 μM Bic, that induced spontaneous synchronous bursts in both field and whole cell recording system. These spontaneous activities always originated in the sSC and spread to the dSC. These findings indicate that the cells located in ventral portion of the sSC should initiate these spontaneous synchronous burst. Among the candidates, WFV cells, which have large dendritic trees receiving the abundant visual inputs in the dorsal portion of SGS (Endo et al., 2008), are most likely. In a previous study, which analyzed the timing of initiation of synchronous depolarization between the pairs of neurons located in the different layers of the SC, it has been shown that the spontaneous depolarization in WFV cells preceded those in the SGS and SGI neurons (Saito and Isa, 2005). Recently, it was found that WFV cells have hyperpolarization-activated cyclic nucleotide-gated (HCN) channels of larger amplitude and faster activation kinetics compared with other cell types in the sSC (Endo et al, 2008). To clarify the possible contribution of WFV cells in generation of spontaneous synchronous bursts, the effect of I_h blockers was investigated in the present study. The results showed that the I_h blocker suppressed generation of the spontaneous synchronous bursts, supporting the hypothesis that the WFV cells are the origin for the propagation of activity in the SC. We have tried to test this hypothesis directly by current injection to the recording WFV cell and record field potential simultaneously weather the current injection to a single WFV can evoked the burst responses in field recording or not. The numbers of WFV cells were tested (> 40 cells), the two cell demonstrated the positive results (data not shown). However, the

evoked responses appeared only about 20% of current injection trials. It is still not clear weather the direct stimulation to the WFV cells can initiate the burst that spread in the large populations of neurons or not. Further studies are required to prove this hypothesis. The WFV cells were shown to be motion-sensitive (Major et al., 2000). The strong linkage of the WFV cells to burst generation mechanism in the SC local circuits might represent the requirement of implementing the quick response system to moving objects in the wide environment.

In addition, we have investigated the responses elicited by the photostimulation system in the various depth of the SC coronal slice (Fig. 3.1). Surprisingly, the SGI stimulation exhibited the less spread of activity than SGS or SO stimulation. This suggests that the amplified network in the sSC is necessary for the wide spread of activity in the dSC. In this case, I_h blocker does not prevent the amplifying mechanism (unpublished observation). Therefore, many questions are arising as to the neural substrate that is employed for such signal amplification mechanims and how it works.

Figure Legends

Figure 3.1 The field potential responses evoked by the photostimulation to the different layers. ***A,*** The position of multi-electrodes on a slice. The boundaries of the slice and between layers (the sSC and the dSC) are indicated by white lines. The red circles show the stimulation sites in various layers where the laser beam was applied, number 1 in SGS, 2 in SO, 3 in SGIa, 4 in SGIb layers. ***B,*** Computed color images of field potentials evoked by the uncaging-photostimulation system. The location of stimulations are indicated by the white circles.

Figure 3.2 Spread of activity of spontaneous burst. ***A***, The coronal slice of the SC overlying the multielectrode array. White lines show the boundaries of slice and border between the sSC and dSC layers. ***B***, A representative spontaneous burst recorded by the 64-channel field potential recording systems. The pale green lines indicate the boundaries as white lines in (A). ***C***, The activity of the channel indicated by the blue square is shown with the 50-sec recording. ***D, E***, The computed color images of field potential from (D) are shown in (E). 500-ms duration shown in (E) corresponds with the duration indicated by a bar in (D). ***F***, the largest amplitudes of negative field potential at any given time in (E) are shown by the small squares. The black line indicates the path of center of the largest potential spread. The orange lines indicate the boundaries as white lines in (A).

Figure 3.3 ZD 7288 blocked the initiation of spontaneous burst. ***A***, The coronal slice of the SC overlying the multielectrode system. The white line shows the boundaries between the sSC and the dSC layers. The whole cell recording was performed near the planar electrode in blue square. ***B***, The representative spontaneous burst recorded by the 64-channel field potential recording system. ***C***, A representative spontaneous burst event from whole cell and field potential recording systems recorded simultaneously on a point in the sSC, is shown in red and blue traces, respectively. ***D***, The spontaneous burst from both recording systems in (C) is eliminated by the bath application of 50 μM ZD7288.

Figure 3.1

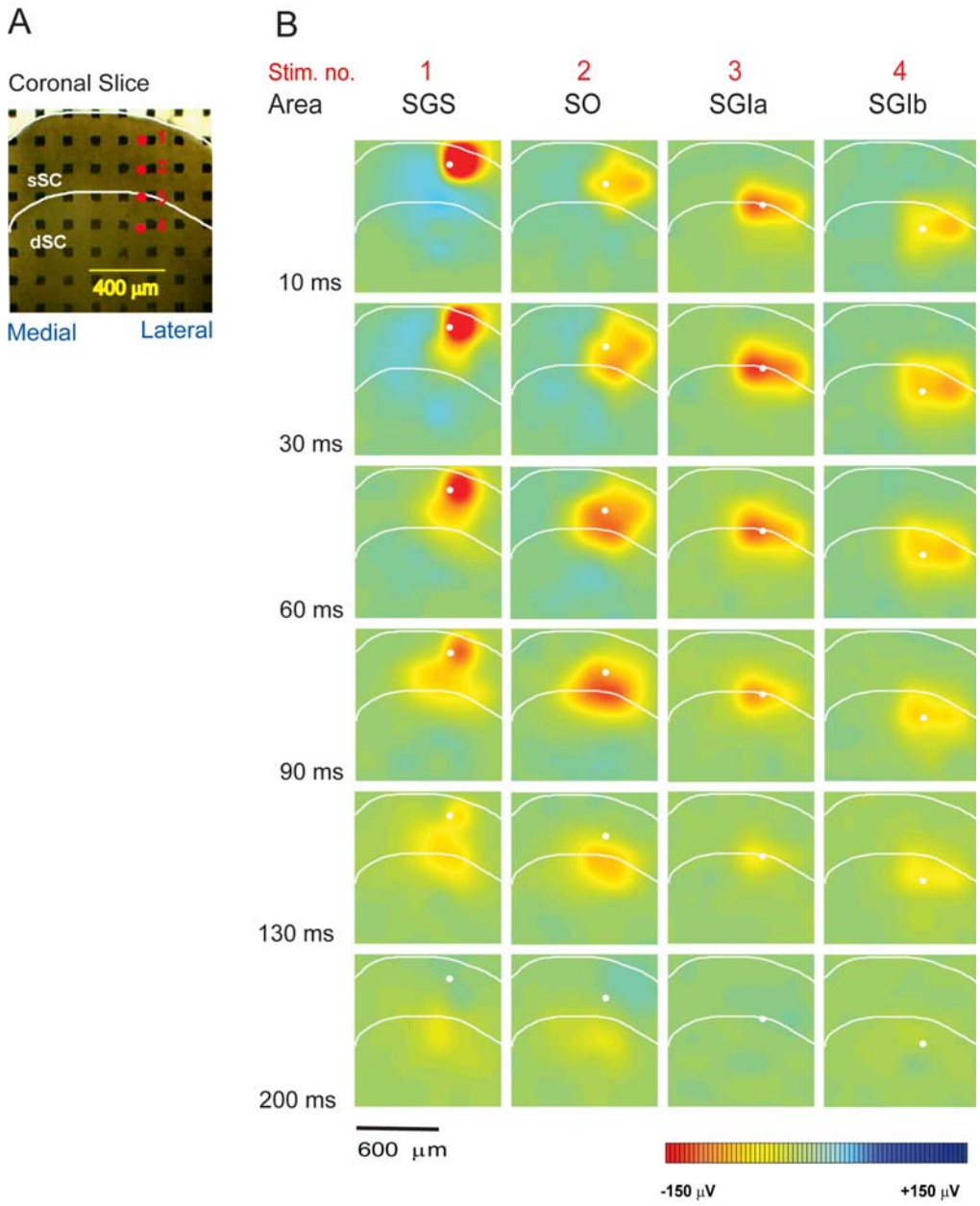
A
Coronal Slice
sSC
dSC
400 µm
Medial
Lateral
B
Stim. no.
1
2
3
4
Area
SGS
SO
SGIa
SGIb
10 ms
30 ms
60 ms
90 ms
130 ms
200 ms
600 µm
-150 µV
+150 µV

Figure 3.2

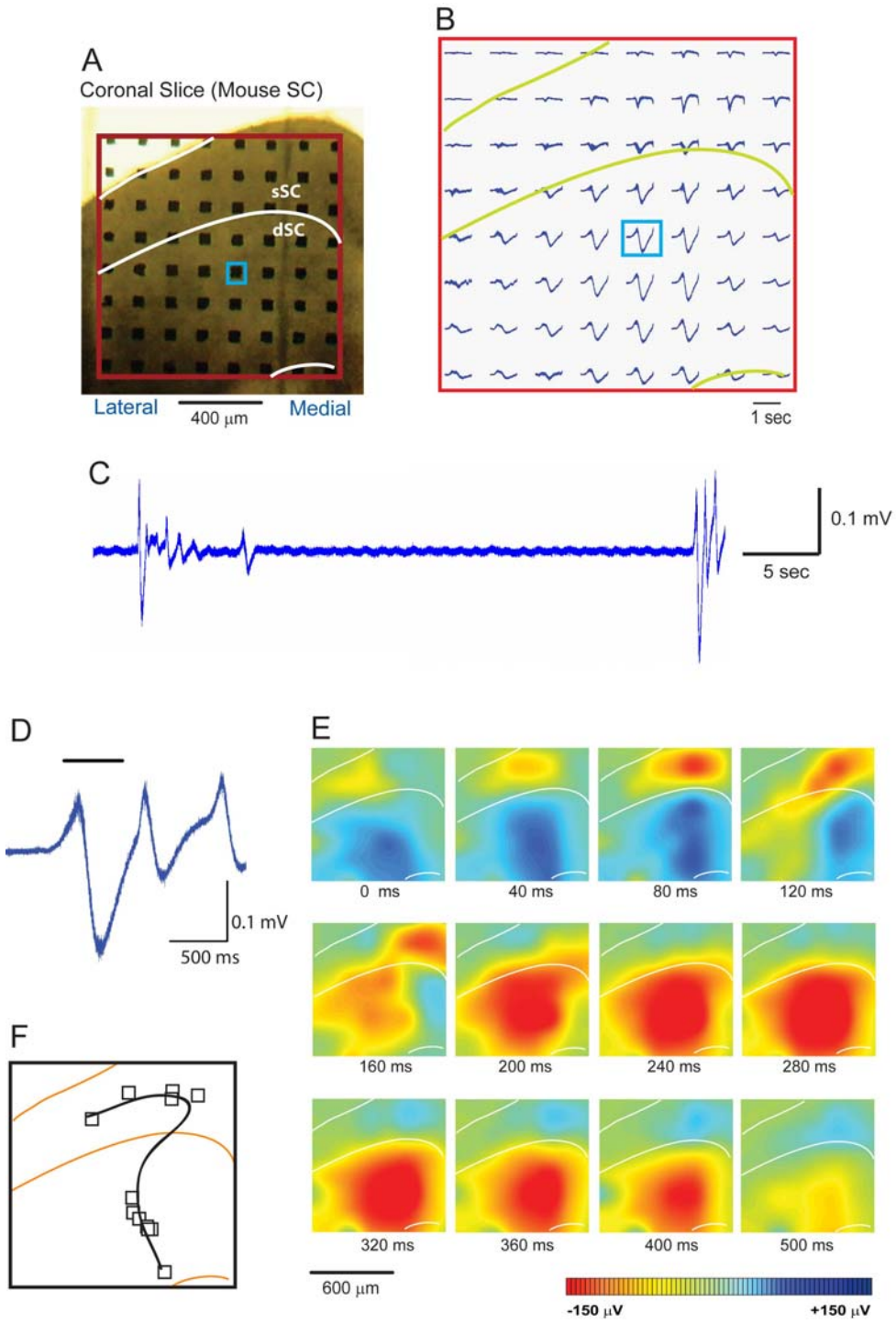
A
Coronal Slice (Mouse SC)
sSC
dSC
Lateral
400 μm
Medial
B
1 sec
C
0.1 mV
5 sec
D
0.1 mV
500 ms
E
0 ms
40 ms
80 ms
120 ms
160 ms
200 ms
240 ms
280 ms
320 ms
360 ms
400 ms
500 ms
600 μm
-150 μV
+150 μV
F

Figure 3.3

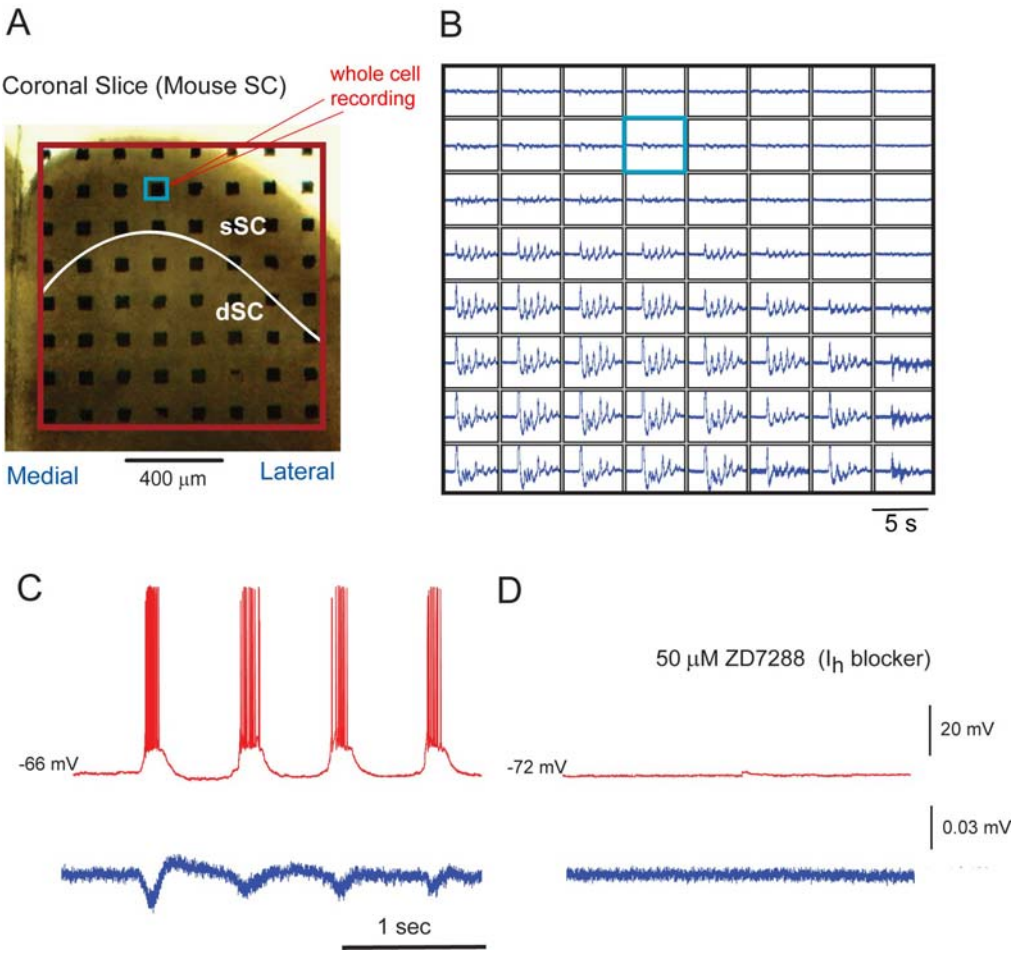
A
Coronal Slice (Mouse SC)
whole cell recording
sSC
dSC
Medial
400 μm
Lateral
B
5 s
C
-66 mV
1 sec
D
50 μM ZD7288 (Ih blocker)
20 mV
-72 mV
0.03 mV

Part IV

The lateral connections in the superficial layer

Introduction

The visual field contains the information that exceeds capacity of the human brain to process at the same time. At any given time, only objects in a small area around the fovea are selected to be processed and used for perception and control of behaviors. Such act of the brain is called "selective visual attention" (Desimone and Duncan, 1995). Attention is an old concept in perception (Tsotsos, 1992) and crucial mechanism for survival of the organism in the natural environment. In the sensory processing network, it works as a bottleneck in sensory processing that allows only a small part of sensory input in the environment pass through the detailed processing (Itti and Koch, 2001). Visual attention involves an intricate network of brain areas, and targeted in many fields of sciences such as psychology, neurophysiology, and computational neuroscience.

The first explicit computational model of bottom-up attention is proposed by Koch and Ullman in 1985. The 'saliency map', an important concept for many models of visual attention, is a key part in that model for implementing parallel search in natural visual field. It pools the different features map of the input images that are decomposed by several pre-attentive mechanisms, which operate in parallel, across the space of visual topography. The contents of saliency map compete in 'winner-take-all' fashions to establish the most salient location that directs the focus of attention, whereas 'inhibition of return' suppresses the last attended location (Itti and Koch, 2001). The model of saliency map is supported by sparse experimental evidences. Recording neurons in lateral interparietal (LIP) area demonstrated that only the most salient or behaviorally relevant

objects being strongly represent in this area (Gottlieb et al., 1998). The positron emission tomography study provided the relationship between the pulvinar activity and attention task in human (LaBerge and Buchsbaum, 1990). Until now, multiple areas are suggested to encode stimulus saliency in the visual system in monkey, including LIP of the posterior parietal cortex, the frontal eye fields, the inferior and subdivisions of pulvinar and the SC (Itti and Koch, 2001).

The SC is a crucial node in oculomotor network (Fecteau and Munoz, 2006). It receives convergent afferents of visual information from many regions at the subcortical and cortical levels. The SC, which functions as an integrative center linked between cortical network and brain stem premotor circuit, therefore, is proposed to be one of integrative centers in deployment of visual attention (Trappenberg et al., 2002).

The competitive interaction of neural circuit of visual attention models was proposed to be mediated by the short-range excitation that increases the activity in closer neurons and long-range inhibition that decreases the activities in the further neurons (Van Opstal and Van Gisbergen, 1989). If models of competition of visual scenes could be encoded in the SC neural network, the lateral connection of the SC neurons should demonstrate the center excitation-surround inhibition which is mediated by wider inhibitory than excitatory connection in the SC local circuit. Lee and Hall (2006) have reported that that pattern of response was not found in the SGI when they investigated in the rodent parasagittal and coronal slices by photostimulating system. They could not find reliable strong inhibitory response in the neurons located in the remote distance, 500 μm, from the stimulation site. Therefore, the 'winner-take-all' hypothesis is not known weather it mediated the target selecting process in the SC or not.

In this Part, the lateral connection within the local circuit of the SC that is crucial to understand the mechanism underlying the competitive process in the SC was studied. We introduced the new in vitro experimental system by cutting the horizontal slice of the SC combined with the 64-channel multielectrode system. The horizontal slice can preserve much more lateral network than the coronal or parasagittal slices (Fig. 4.1*C-D*), while the new multielectrode stimulating system permit us to change the location of stimuli easily and systematically. The horizontal slice that was comprised of the SGS-SO layers were stimulated by the planar multielectrode on the SO side and recorded by the whole cell patch clamp recording in the SGS neurons on the opposite side of slices. The stimulations in various distances simulated the incoming sensory input to the SGS neurons from the retina or visual cortex via the fibers in the SO which enters the SGS perpendicularly and issue arbolizing axons in the confined region of the SGS (Sachs and Schneider, 1984). The integrated area of either postsynaptic potential or current was calculated to compare the amplitude of intracellular responses evoked by the stimulating electrodes located proximally and distally to the recorded cell. The relationship between the amplitude of response and the distance between the stimulation and recording exhibited the Mexican-hat-shaped curve when high frequency repetitive stimuli was applied, which indicated implementation of the central excitatory-distal inhibitory connection in the local circuit of the sSC. Moreover, interestingly, we found that the temporal pattern of the excitatory and inhibitory responses are a crucial factor for synaptic integration.

Materials and Methods

The experimental protocol was approved by the Animal Research Committee of the National Institute of Natural Science. All efforts were made to minimize both the suffering and number of animals used in this study.

Slice preparations

The procedures for slice preparation were described in **Part II**. Briefly, horizontal slices (250 μm thick) of the SC were prepared from C57BL/6 wild type or GAD67-GFP knock-in mice, 16- to 20-day-old. The animals were deeply anesthetized with ether and decapitated. The brains were quickly removed and submerged in ice-cold modified Ringer solution for 4-6 min. Slices were cut with a Microslicer (DTK-2000, Dosaka EM, Kyoto, Japan) in the horizontal direction with a small declining angle in lateral side to fit the curve of the SC shape (Fig.4.1*A*), and then the remaining brain blocks were slice in coronal direction. These coronal slices (Fig. 4.1*B*) were examined under microscope before starting the recording experiments to confirm the cutting angle and layer components of the horizontal slice. Horizontal slices were incubated in standard Ringer solution at room temperature for more than 1 h before recording.

Stimulations with multielectrode array

The multi-channel recording system (MED64 system Panasonic) was employed to stimulate the slice in various locations from the recorded neuron. The Slices were placed on the center of the MED probe, 8 × 8 array, and continuously perfused with the standard Ringer's solution at 33-34°C. The slices were then left for 15 min to sufficiently attach to the electrode array. Single planar microelectrode of the 64 available was selected by the 64-switch box and used for stimulation. Biphasic current pulses (0.1 ms negative pulse

and 0.1 ms positive pulse) were initiated by the data acquisition software (MED64 Condutor 3.1TM, Panasonic, Japan). The current intensity was adjusted in each neuron to elicit the appropriate responses; the intensity that evoked 50-80% of maximal amplitude of EPSP or EPSC at the nearest electrode, visually guided, was used for all experiments of each cell.

Recordings and analysis

Whole-cell patch clamp recordings

Electrophysiological recording. The procedures for whole-cell recording were described in **Part II**. Briefly, whole-cell patch-clamp recordings were obtained from the neurons in the SGS and SGI by visual control of patch pipettes. GFP-negative neurons located in the central part of the slices were selected using fluorescent optics, and then a whole-cell configuration was obtained using bright-field optics. In current clamp recording mode, patch pipettes were filled with a 'K-gluconate' internal solution containing (in mM) 150 K-gluconate, 2 $MgCl_2$, 4 Na_2ATP, 0.3 Na_3GTP, 0.2 EGTA, 10 HEPES, and 0.1 spermine, pH 7.3. Whereas, in voltage clamp recording mode, patch pipettes were filled with a 'Cs-gluconate' internal solution containing (in mM) 120 CsOH, 10 EGTA, 2 $MgCl_2$.6H2O, 2 Na_2ATP, 10 Hepes, 0.3 Na_3GTP and 0.1 spermine, pH 7.3. To stain the recorded neurons, biocytin (5 mg/ml; Sigma, USA) was dissolved in the solution. In all experiments, we added QX-314 (2.5 mM; Sigma, USA) to the intracellular solution to block the action potential responses. The resistance of the electrodes was 4–8 MΩ in the Ringer's solutions. The actual membrane potentials were corrected by the liquid junction potential of –10 mV. The neurons were recorded at their original membrane potential, -55 to -65 mV, in the current recording. In contrast, the cell membranes were clamped at 0 or -80

mV in the voltage clamp recording. The whole cell recordings used a patch clamp amplifier (EPC-7, Heka, Germany) connected through a Digidata1322A analogue/digital interface card (Axon Instrument, USA). The data were acquired using a pClamp system (pClamp 8.0, Axon Instruments, USA).

Histological procedures. After whole cell recordings, slices were fixed with 4% paraformaldehyde in 0.12 M phosphate buffer (pH 7.4) for more than two days at 4°C. After fixation, biocytin-filled neurons were visualized by the ABC method. Details are described elsewhere (Isa et al., 1998).

Data analysis. Eight sweeps of intracellular responses from each stimulation protocol were averaged by using a pClampfit 10.2 software (Axon Instruments, USA). These averaged responses were used for demonstration in figure 4.2*B* and for calculation of the integrated area which have been done by running a MatLab 7.0.4 (Mathworks, USA) script file. In brief, first, the stimulus artifacts detected by their sharp rise-fall characteristics were removed. Then, the area under the curve was integrated within the desired period, 50 ms or 200 ms in cases of single pulse or multiple pulses, respectively. The net areas were resulted from subtracting the negative value of the IPSP area from the positive value of EPSP area. The color images of intracellular response (Fig. 4.4*B*-*E* and Fig. 4.5*B*-*F*) were plotted by the net areas that transformed to be the colors and mapped those colors to the corresponding electrodes that evoked the responses.

Results

4.1 Short-range excitatory and long-range inhibitory connection in stimulus frequency dependent manner

The horizontal slice comprised SGS and SO layers were placed on the array of microelectrodes attached the SO layer toward the planar electrodes (Fig. 4.2*A*). The EPSPs or IPSPs in the SGS neuron, marked in green circle, from whole cell recording were elicited by stimulations from one of the multielectrodes attached to the side of the SO layer. The effects from six selected stimulating electrodes are indicated as the pale blue squares labeled as number 1-6 in rostro-caudal direction. Figure 4.2*B* indicates the EPSPs or IPSPs evoked by stimulation at electrode No. 1-6. The intracellular responses of 100-ms repetitive stimuli at three different frequencies, 10 Hz (red), 100 Hz (pink) and 200 Hz (blue), are shown in top, middle and bottom rows, respectively. The integrated area of evoked intracellular potentials was plotted in figure 4.2*C* against the distance between each stimulating electrode and the recorded neuron. The positive or negative values of integrated area indicate that the EPSP or IPSP dominated in the responses from the respective stimulating electrode location. According to figure 4.2*B* and 4.2*C*, the stimulating electrode, proximal to the neuron, evoked the dominant EPSPs resulting in the positive values of the integrated area that increased by increasing of the stimulus frequency. On the other hand, the more distal electrodes evoked the dominant IPSPs increasing negatively with higher stimulus frequencies on both rostral and caudal sides. Then, both excitatory and inhibitory responses could not be evoked, when the most distant electrodes, no. 1 and 6, were stimulated.

4.2 The Mexican-hat-shaped curve of response-distance relationship

As shown in figure 4.2*B*, the center-surround competitive interaction was found explicitly when high frequency repetitive stimuli were applied. We then analyzed the evoked responses that depended on the distances between the stimuli and the neurons with two different stimulus protocols, single pulse versus multiple pulses (200 Hz, 50 ms). As shown in figure 4.3, the excitatory effect was strong when the site of stimulation was close to the cell. The excitatory responses were prominent when stimulations were initiated at the closest electrodes, at the 0 μm in the graphs. The excitatory connections was found within the diameter of approximately 300 μm. Then this "excitatory area" was surrounded by the area from which inhibition was induced. As shown in figure 4.3*A*, the responses were not symmetrical along the rostrocaudal direction; since the lateral inhibition was found only on the caudal side and the effect was always excitatory on the rostral side. We suggested that this asymmetrical shape might caused by the complication of stimulating the fibers of passage. The majority of horizontal passing fibers in the sSC are the optic fibers that arrive from the rostral pole and distribute caudally in the SO layer. There was a high possibility that the activated fibers sent the signal rostro-caudally. This short-cut network might have built-up the excitatory response in the recorded cell and masked the lateral inhibition. On the other hand, nearly symmetrical responses were observed along the latero-medial axis (Fig. 4.3*B*), which supported our suggestion.

4.3 Excitation is surrounded by inhibition

By transforming the intracellular evoked responses from individual stimulating electrodes into the color images, two-dimensional connection map onto the recorded SGS neuron, indicated by the green circle, can be constructed as shown in figure 4.4.

During 50-ms repetitive stimuli, excitatory and inhibitory responses were evoked in different spatial and temporal manners. The excitation appeared shortly after the first stimuli in case of stimulation with the electrode next to the cell (Fig. 4.4*B*), whereas the inhibition gradually built up for stimulation at distant locations (Fig. 4.4*C*-*E*). Both excitatory and inhibitory areas were expanded on application of train stimuli, which indicated that those repetitive stimuli could recruit larger number of neurons, particularly from remote area, than the single stimulus. However, at the period of 50-51 ms after the first stimulus (Fig 4.4*E*), the inhibitory input reached its maximal amplitude, while the excitatory input was getting weaker. The results suggest that SGS neurons receive the strong excitatory signal with the short latency, shorter than 5 ms, mainly by direct connections, whereas the inhibitory signal is mainly sent from distant regions by either the long projections with short latency or through polysynaptic connections with long latency. It should be noted that the closest electrode was not necessarily evoked the largest response, and the center of excitatory input field often shifted from the location of the cell body. The dendritic field might be more fitted better with this input field than the soma, which should be examined in future studies.

4.4 Separated Excitatory and Inhibitory input

The strong inhibitory input from remote areas was shown in figure 4.3 and 4.4; however, it was still questionable about the existence of short-range inhibitory connection because of mixture with the excitation. To investigate the organization of excitatory and inhibitory networks, it is necessary to explore both input signals to the SGS neurons separately. The voltage clamp recording in two different holding potential enables us to examine the excitatory input at -80 mV, the equilibrium potential of chloride in our

system, and the inhibitory input at 0 mV, the equilibrium potential of glutamate receptors, in the same neuron.

The color images in figure 4.5 show the integrated area of excitatory postsynaptic currents (EPSCs) for each of 10-ms period during the initial 50 ms after the single pulse stimulus, recorded at -80 mV on the left column, and the integrated area of inhibitory postsynaptic currents (IPSCs) recorded at 0 mV evoked by the 200 Hz repetitive stimuli on the right column, respectively. Both excitatory and inhibitory responses reached the maximum amplitude during the period of 10-20 ms (Fig. 4.5*C*), and then gradually declined (Fig. 4.5*D*-*F*). However, the temporal rising and declining profiles of those two responses were different; the excitation decreased earlier than inhibition. As shown in figure 4.5*E* and *F*, the areas of excitatory input field became smaller than those of inhibitory input field during 30-40 ms and 40–50 ms period. From these results, the short inhibitory connection was found, but it was weaker than the excitatory connection and appeared to be dominated by excitation.

Discussion

The experimental results in awake behaving monkeys indicated that the microstimulation and pharmacological application of the SC can alter the ongoing trajectories of saccadic movements (Dorris et al., 2007; Carello and Krauzlis, 2004; McPeek and Keller, 2002; Quaia et al., 1998). Subthreshold microstimulation resulted in the increase of the distractor-directed saccade error toward to the location of stimulating electrode (Dorris et al., 2007). This indicates the role of the SC in the competitive process involved the selection and execution of saccades. However, it is still not known weather the competitive integration between sensory and preparatory signals arises through local excitatory and distant inhibitory connections implemented in the SC local circuits or through the external connections that impinges on the SC. There are *in vitro* and *in vivo* experiments that support either of these possibilities (Munoz and Istvan 1998, Lee and Hall 2006). However, those experiments have studied the neuronal organization of the intermediate layer. We have introduced the new *in vitro* experimental system in which the lateral connections are preserved in the sSC horizontal slices, and stimulations are applied to various locations on the optic fibers systematically. Our results explicitly demonstrate the distant inhibitory connection in the local circuit of the sSC. However, the stimulations located rostrally to the recording neurons did not evoke the inhibitory responses as observed on the caudal side. The optic fibers that run in the rostro-caudal direction in the SO layers might be stimulated on the rostral side of horizontal slices. It is possible that the electrical stimuli activated the passing fibers that sent the excitatory signal to neurons located on the caudal direction apart from visually closest electrode. That means the rostrally distant electrode might directly activate the recording neuron

with excitatory short connection. This complication of electrical stimulation should be then examined by using the laser uncaging photostimulation system that activates only the neurons at the uncaged area.

The neural network mediating the nearby excitatory and distant inhibitory connections was investigated in the voltage clamp recording. The multiple stimuli, 200 Hz, were tested in the recording neuron with two different holding potentials, at -80 mV and 0 mV, to examine the excitatory and inhibitory connection, respectively. The color images demonstrating the temporal profile of responses extended on the stimulating electrode grid indicate that the both excitatory and inhibitory network have both short- and long-range connections. The nearby excitatory and distant inhibitory connections that are shown in figure 4.4 are subtracted results between those connections. The excitatory connections are stronger in the central area, while the inhibitory connections in the surrounding area. The different temporal patterns of those connections should also underlie their competitive relationship. As shown in figure 4.5, the excitation rises earlier already during the first 10 ms, and then declines with faster decay time than inhibition, which affects to the distant location that inhibition still relatively strong. Therefore, we suggest that the distant inhibitory response is mainly contributed by the slower desensitization of the inhibitory synaptic connections than excitatory ones in the remote location.

Figure Legends

Figure 4.1 Horizontal slice. ***A,*** The schematic drawing indicates the cutting plane of horizontal slice with arrangement of stimulating and recording system from the coronal view. The red arrows in SO layer show directions of stimuli that are initiated by the 64-channel MED system. ***B,*** The coronal slice cutting from the remaining brain block which the horizontal slices were made. ***C,*** The fresh horizontal slice of the right SC overlying a multielectrode array. ***D,*** Map of visual field on the surface of mouse SC (adapted from Dräger and Hubel, 1975)

Figure 4.2 The frequency dependent responses. ***A,*** The horizontal slice overlying an electrode array. The green circle indicates the location of recorded SGS neuron. The electrical stimulations to the cell were initiated from each of six electrodes in the blue square. ***B***, The evoked EPSP or IPSP from the stimulation from electrode number 1-6 in figure A are shown in three rows of three stimulus frequencies, 10 Hz (red), 100 Hz (pink), and 200 Hz (blue), from top to bottom row, respectively. The durations of stimulus were kept constant at 100 ms. ***C,*** The integration of EPSP (positive value) and IPSP (negative value) during 0-200 ms after starting stimulation were summarized and plotted on the distance axis that the closest electrode to the cell was set to be zero. Three different stimulus frequencies are shown in colors as mentioned above.

Figure 4.3 The Mexican-hat-shaped graph of response-distance relationship Percent of maximal responses were plotted on the distance between t the stimulating electrode to the cell closest electrode. Two stimulus protocols were tested, single pulse (pink) and 11 pulses/ 200 Hz (dark blue). ***A***, the rostrocaudal direction (n = 8-12). ***B,*** the lateromedial direction (n = 6-10). All data expressed as means ± SEM.

Figure 4.4 The color images of response mapped on the stimulating electrode array. ***A,*** The horizontal slice overlying an electrode array. The green circle indicates the location of recorded neuron. ***B-E***, 1-ms integrated areas of EPSP or IPSP evoked in the SGS neuron at the green circle were computed to be colors, positive values are red and negative ones are blue, and mapped on the location of each stimulating electrode. The 200 Hz stimuli were applied in 50-ms duration. Only electrodes marked with white squares were tested.

Figure 4.5 The color images of excitatory and inhibitory response mapped on the stimulating electrode array. ***A***, The horizontal slice overlying an electrode array. The green circle indicates the location of recorded neuron. ***B-F***, The whole cell voltage clamp recording was performed in the SGS neuron located at the green circle with two holding potential, -80 mV (left column) and 0 mV (right column).10-ms integrated areas of EPSC or IPSC were computed to red and blue colors, respectively, and mapped on the location of each stimulating electrode. The 200 Hz stimuli were applied in 50-ms duration.Only electrodes marked with white squares were tested.

Figure 4.1

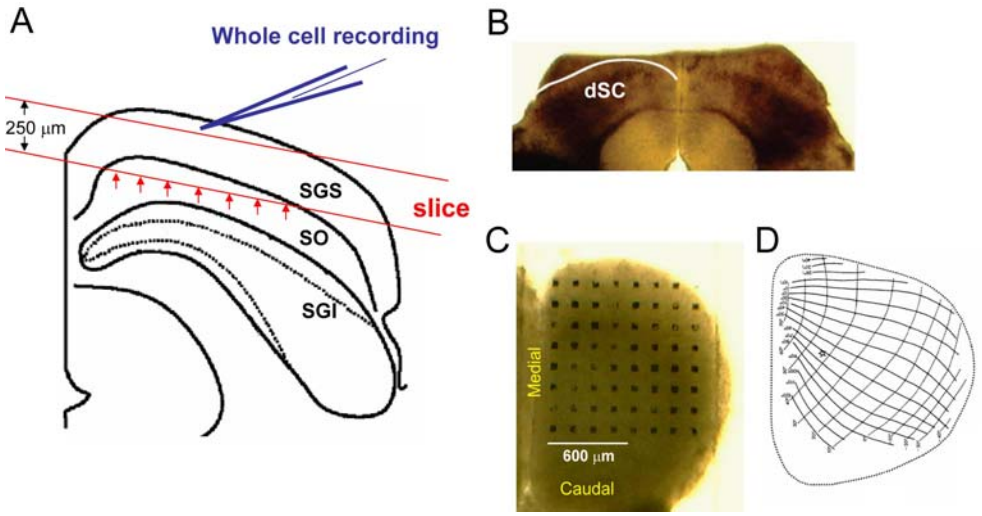
A
Whole cell recording
250 μm
SGS
SO
SGI
slice
B
dSC
C
Medial
600 μm
Caudal
D

Figure 4.2

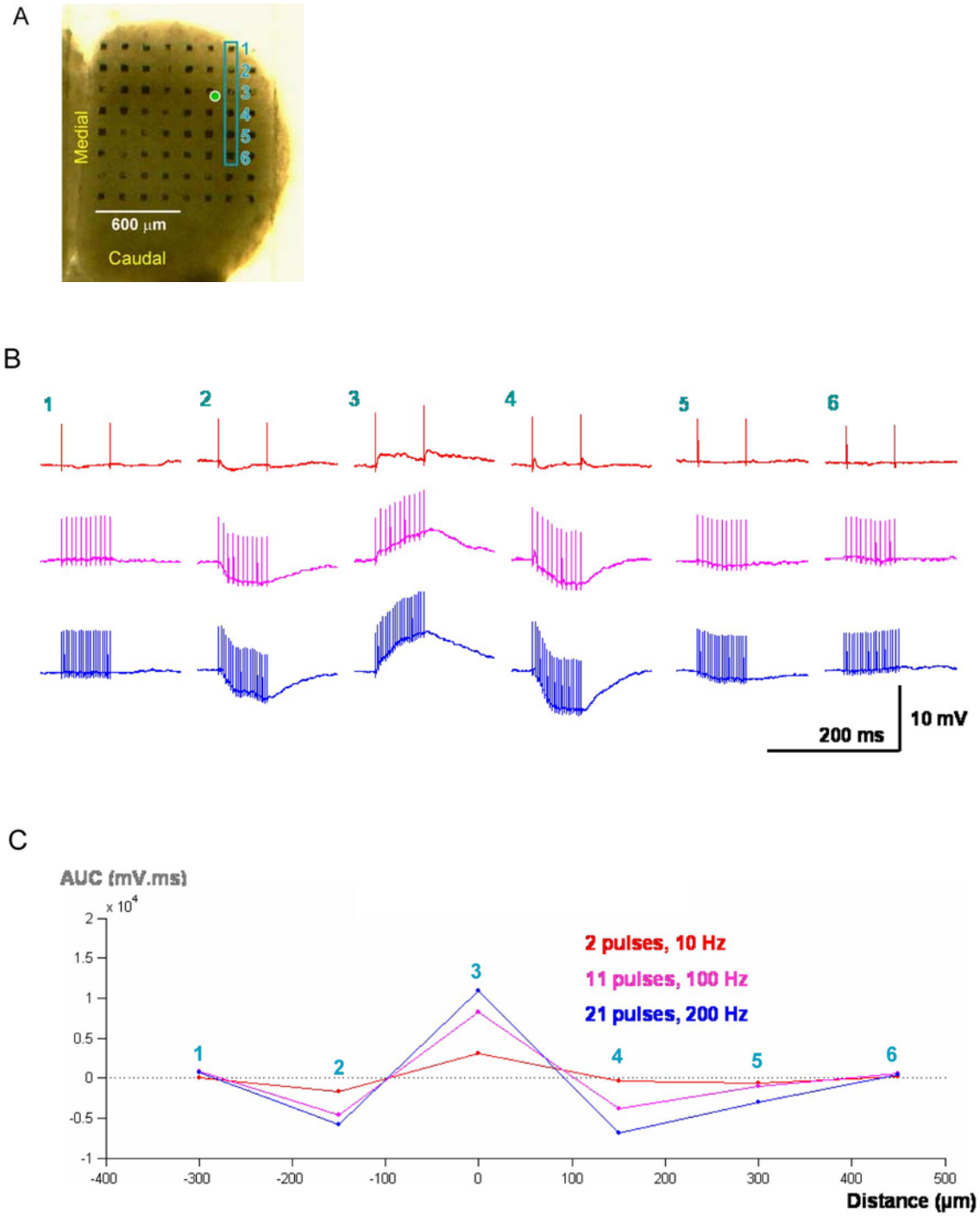
A
Medial
1
2
3
4
5
6
600 µm
Caudal
B
1
2
3
4
5
6
200 ms
10 mV
C
AUC (mV.ms)
x 10^4
2
1.5
1
0.5
0
-0.5
-1
-400
-300
-200
-100
0
100
200
300
400
500
Distance (µm)
2 pulses, 10 Hz
11 pulses, 100 Hz
21 pulses, 200 Hz
1
2
3
4
5
6

Figure 4.3

A. Rostrocaudal direction

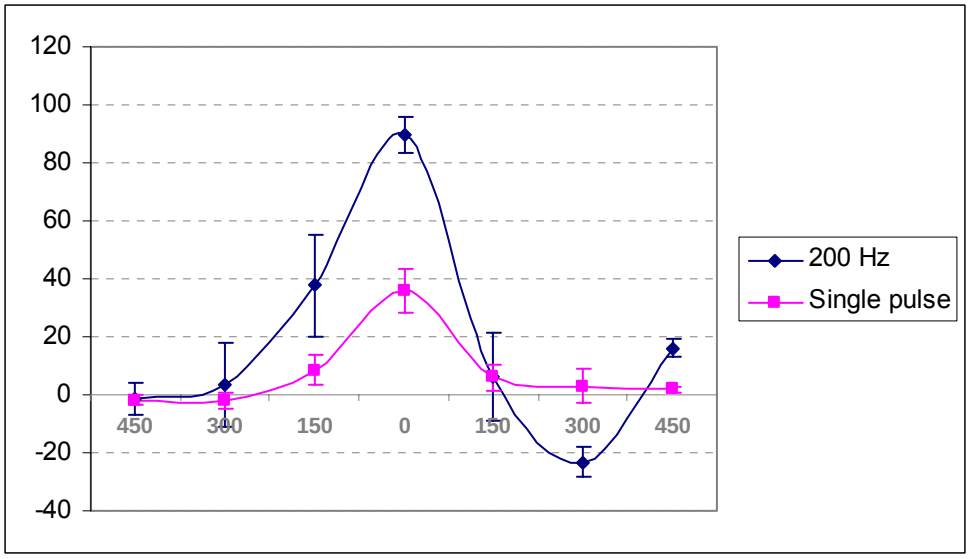

B. Lateromedial direction

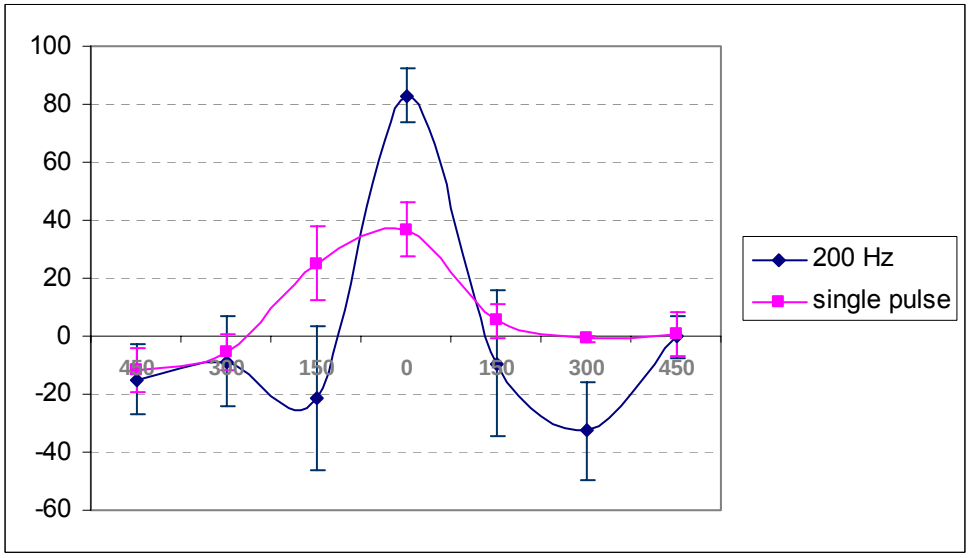

Figure 4.4

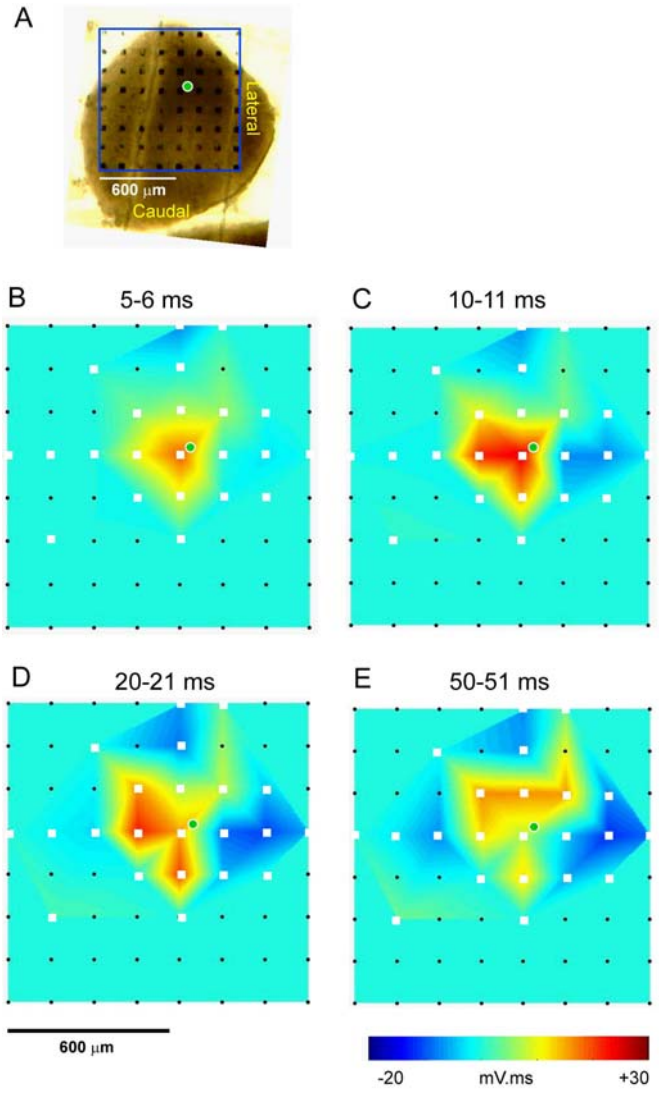
A
Lateral
600 μm
Caudal
B
5-6 ms
C
10-11 ms
D
20-21 ms
E
50-51 ms
600 μm
-20
mV.ms
+30

Figure 4.5

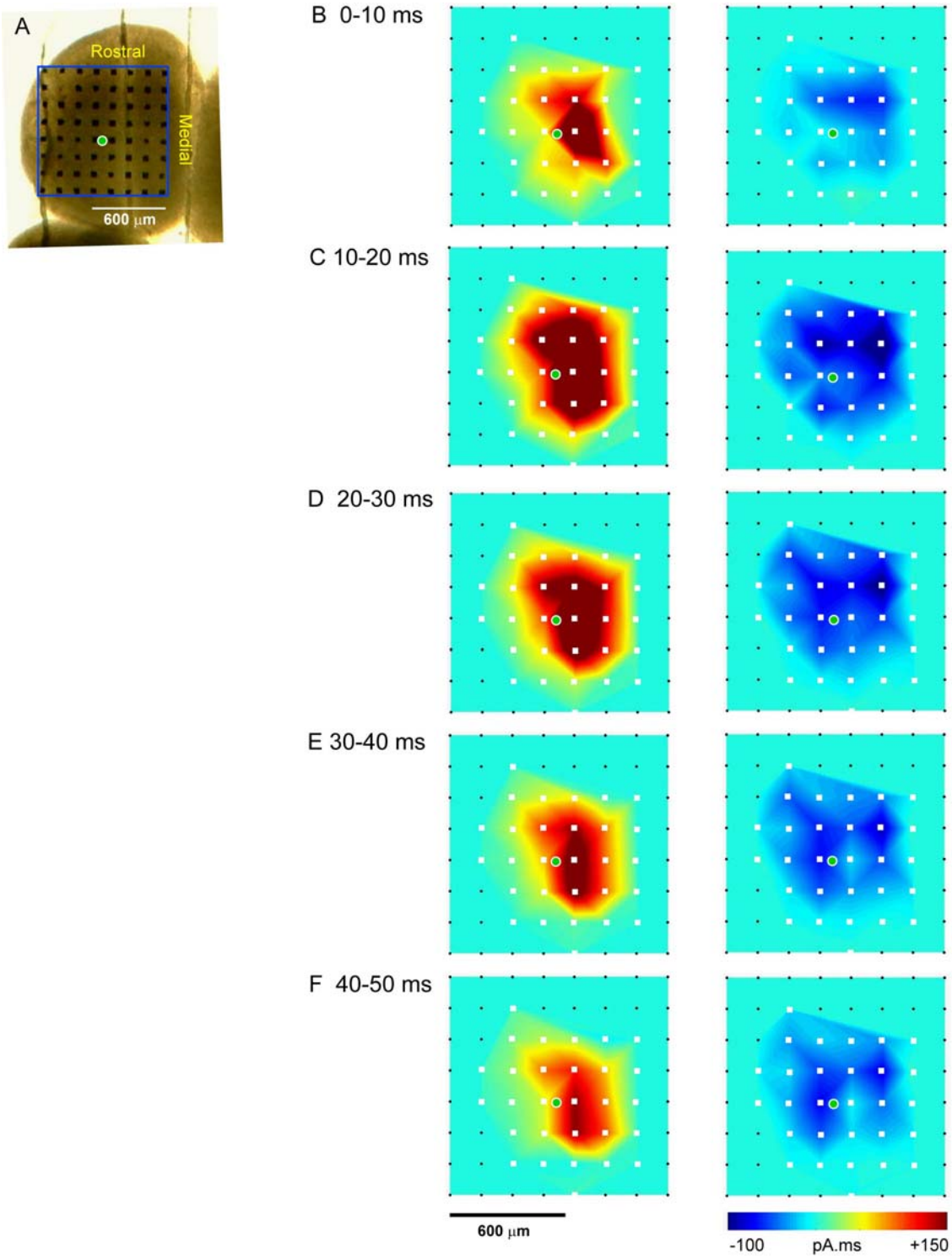
A
Rostral
Medial
600 μm
B 0-10 ms
C 10-20 ms
D 20-30 ms
E 30-40 ms
F 40-50 ms
600 μm
-100
pA.ms
+150

Part V

General Discussions and Conclusions

The main goal of our study is to clarify the neuronal connection and signal processing within the local circuit of SC. We have introduced the new planar multi-electrode stimulating/recoding system that deals with the populations of neurons to overcome the previous limitation of sparse-sampling recording. This system records field potential simultaneously from 64 locations, 8x8 arrays with 150 μm inter-electrode space. Moreover, while recording the field potentials in slice, it is possible to perform whole-cell patch-clamp recording simultaneously. Working with these two recording systems allow us to investigate the neural network of large populations of neuron, while precisely study the intracellular postsynaptic potentials/currents. However, In **Part II**, the disadvantages of 64-channel multielectrode system are characterized. The positive potential from this recording system did not indicate that the neurons are concurrently hyperpolarized, but simply indicated the current source of activities in the negative-response location. The field potential analysis did not always clearly illustrate the onset of activity, which seems to be the most important limitation of this system. Nevertheless, the multichannel field potential recording system should be a powerful tool for studying spatio-temporal profiles of the spread of activity in the local circuit of the SC.

The interlaminar and intralaminar circuits of the SC are described in this paper. In **Part II**, the spread of activity from the sSC stimulation in the presence of $GABA_A$ antagonist was indicated the existence of visuomotor pathway, direct link between the sSC and the dSC, as found in previous *in vitro* studies. The signal arisen in the sSC propagated in non-linear amplification, particularly in the dSC. The large area of propagation covering

almost entire dSC area shows that the motor vector occurring in the dSC preceding the orienting movement is recruit a large population of dSC neurons, while the center of mass is moving ventrally. We have tested the effects of stimulation in different layer in **Part III**. The photostimulating system, emitted the laser beam to a specific location to release glutamate to activate the desired population of neurons, was used for avoiding complication of passing fiber stimulation. Interestingly, it is found that the dSC stimulation evoked the less spreading burst than that evoked by the sSC stimulation. To explain the mechanism underlying this finding, the neuronal circuit of the visuomotor pathway should be studied in more details. However, the hypothesis of amplification circuit located in the sSC is in agreement with our findings in the spontaneous phenomena. In **Part III**, the spontaneous burst activity was occurred when the slices were exposed to the external solution containing low Mg^{2+} and Bic. This spontaneous activity is proposed to share the basic mechanism with the presaccadic burst in the dSC. The synchronous spontaneous bursts always originally occurred in the sSC with a variety of locations in this layer. Furthermore, these bursts disappeared when the I_h blocker was applied. These finding support the hypothesis that the WFV cells is the origin of spontaneous burst. Later, we moved to the lateral connection in the sSC in **Part IV**. The horizontal slice comprising SGS and SO layer was prepared and placed on the planar electrodes, while the SGS cells were recorded by the whole-cell patch-clamp in the upper side of slice. This method can preserve more the lateral circuit than the coronal or parasagittal slices. Using this new experimental model, the distant inhibitory connection in SGS layer has been shown clearly. The distant inhibition and nearby excitation are the basic concept of many computational model of attention. However, it is not known

weather this relationship is found in the intrinsic circuit of the SC or not. We analyzed the rostrocaudal and lateromedial direction of evoked responses that depend on the distances between the stimuli and the neurons in two stimulus protocols, single pulses and multiple pulses (200Hz, 50 ms). The center-surround competitive interaction was found clearly in the high frequency repetitive stimuli condition. The excitatory responses were prominent when stimulations were initiated at the closest electrodes. It is indicated that those short excitatory connections are surrounded by the long inhibitory projection. The neural network mediating this relationship was investigated in the voltage clamp recording. The multiple stimuli, 200 Hz, were tested in SGS neurons with two different holding potentials, at -80 mV and 0 mV, to examine the excitatory and inhibitory response separately. The color images demonstrating the temporal profile of responses on the stimulating electrode grid indicate that the both excitatory and inhibitory networks have both short- and long-range connections and they are overlapped. The different temporal patterns of those connections also mediate their competitive relationship. We hypothesize that the distant inhibitory response is contributed by the slower desensitization of the inhibitory than excitatory synaptic connections. Although, many investigators devoted their attention to the neural circuit in the SGI, we found that the competitive mechanism is possible to occur in the SGS where a variety of visual inputs arrive.

References

Carello CD, Krauzlis RJ (2004) Manipulating intent: evidence for a causal role of superior colliculus in target selection. Neuron 43: 575-583.

Desimone R, Duncan J (1995) Neural mechanisms of selective visual attention. Ann Rev Neurosci 18: 193-222.

Dorris MC, Paré M, and Munoz DP (1997) Neuronal activity in monkey superior colliculus related to the initiation of saccadic eye movements. J Neurosci 17: 8566-8579.

Dorris MC, Olivier E, Munoz DP (2007) Competitive integration of visual and preparatory signals in the superior colliculus during saccadic programming. J Neurosci 27: 5053-62.

Endo T, Tarusawe E, Notomi T, Kaneda K, Hirabayashi M, Shigemoto R, Isa T (2008) Dendritic I_h ensures high-fidelity dendritic spike responses of motion-sensitive neurons in rat superior colliculus. J Neurophysiol 99: 2066-2076.

Fecteau JH, Munoz DP (2006) Salience, relevance, and firing: a priority map for target selection. Trends Cogn Sci 10: 382-90.

Gottlieb JP, Kosunoki M, Goldberg ME (1998) The representation of visual salience in monkey parietal cortex. Nature 391:481-4.

Hikosaka O, Wurtz RH (1983) Visual and oculomotor functions of monkey substantia nigra pars reticulata. IV. Relation of substantia nigra to superior colliculus. J Neurophysiol 49:1285-1301.

Huerta MF, Harting JK (1984) The mammalian superior colliculus: studies of its morphology and connections. In: Comparative Neurology of the Optic Tectum (Vanegas H, eds), pp 687–773. Plenum, New York.

Isa T (2002) Intrinsic processing in the mammalian superior colliculus. Curr Opin Neurobiol 12:668-77.

Isa T, Endo T, Saito Y (1998) The visuo-motor pathway in the local circuit of the rat superior colliculus. J Neurosci 18:8496-504.

Isa T, Saito Y (2001) The direct visuo-motor pathway in mammalian superior colliculus; novel perspective on the interlaminar connection. Neurosci Res 41:107-13.

Itti L, Koch C (2001) Computaional modeling of visual attention. Nat Rev Neurosci 2:194-203.

Kaneda K, Phongphanphanee P, Katoh T, Isa K, Yanagawa Y, Obata K, Isa T (2008) Regulation of burst activity through pre- and postsynaptic $GABA_B$ receptors in mouse superior colliculus. J Neurosci 28:816-827.

Katsuta H, Isa T (2003) Release from GABA(A) receptor-mediated inhibition unmasks interlaminar connection within superior colliculus in anesthetized adult rats. Neurosci Res 46:73-83.

Koch C, Ullman S (1985) Shifts in selective visual attention: towards the underlying neural circuitry. Hum Neurobiol 4: 219-27.

LaBerge D, Buchsbaum MS (1990) Positron emission tomographic measurements of pulvinar activity during an attention task. J Neurosci 10:613-9.

Langer TP, Lund RD (1974) The upper layers of the superior colliculus of the rat: a Golgi study. J Comp Neurol 158:418-35.

Lee C, Rohrer WH, Sparks DL (1988) Population coding of saccadic eye movements by neurons in the superior colliculus. Nature 332:357-60.

Lee P, Hall WC (2006) An in vitro study of horizontal connections in the intermediate layer of the superior colliculus. J Neurosci 26: 4763-8.

Lee PH, Helms MC, Augustine GJ, Hall WC (1997) Role of intrinsic synaptic circuitry in collicular sensorimotor integration. Proc Natl Acad Sci USA 94:13299-304.

Lee PH, Schmidt M, Hall WC (2001) Excitatory and inhibitory circuitry in the superficial gray layer of the superior colliculus. J Neurosci 21:8145-53.

Lee PH, Sooksawate T, Yanagawa Y, Isa K, Isa T, Hall WC (2007) Identity of a pathway for saccadic suppression. Proc Natl Acad Sci USA 104: 6824-6827.

Major DE, Luksch H, Karten HJ (2000) Bottlebrush dendritic ending and large dendritic field: Motion-detecting neurons in the mammalian tectum. J Comp Neurol 423:243-60.

May P (2006) Chapter11: The mammalian superior colliculus: laminar structure and connections. Prog Brain Res 151: 321-378.

McIlwain JT (1975) Visual receptive fields and their images in superior colliculus of the cat. J Neurophysiol 38:219-30.

McIlwain JT (1982) Lateral spread of neural excitation during microstimulation in intermediate gray layer of cat's superior colliculus. J Neurophysiol 47:167-78.

Meredith MA, Ramoa AS (1998) Intrinsic circuitry of the superior colliculus: pharmacophysiological identification of horizontally oriented inhibitory interneurons.

J Neurophysiol 79:1597-1602.

Mitzdorf U, Singer W (1978) Prominent excitatory pathways in the cat visual cortex (A 17 and A 18): a current source density analysis of electrically evoked potentials. Exp Brain Res 33(3-4):371-94.

Munoz DP and Istvan PJ (1998) Lateral inhibitory interactions in the intermediate layers of the monkey superior colliculus. J Neurophysiol 79(3):1193-209.

Munoz DP, Pélisson D, Guitton D (1991) Movement of neural activity on the superior colliculus motor map during gaze shifts. Science 251:1358-1360.

Munoz DP, Wurtz RH (1993a) Fixation cells in monkey superior colliculus. I. Characteristics of cell discharge. J Neurophysiol 70:559-575.

Munoz DP, Wurtz RH (1993b) Fixation cells in monkey superior colliculus. II. Reversible activation and deactivation. J Neurophysiol 70:576-589.

Munoz DP, Wurtz RH (1995) Saccade-related activity in monkey superior colliculus. II. Spread of activity during saccades. J Neurophysiol 73:2334-2348.

McPeek RM, Keller EL (2002) Superior colliculus activity related to concurrent processing of saccade goals in a visual search task. J Neurophysio. 87: 1805-1815.

Nikitin NI, Isa T (2004) Release from GABAergic inhibition unmasks visual inputs to deeper layer neurons in the superior colliculus in macaque monkeys. Jap J Physiol Suppl.

Oka H, Shimono K, Ogawa R, Sugihara H, Taketani M (1999) A new planar multielectrode array for extracellular recording: application to hippocampal acute slice. J Neurosci Methods 93:61-7.

Özen G, Augustine G J, Hall WC (2000) Contribution of superficial layer neurons to premotor bursts in the superior colliculus. J Neurophysiol 84: 460-471.

Quaia C, Aizawa H, Optican LM, Wurtz RH (1998) Reversible inactivation of monkey superior colliculus. II Maps of saccadic deficits. J Neurophysiol 79: 2097-2110.

Sachs GM, Schneider GE (1984) The morphology of optic tract axons arborizing in the superior colliculus of the hamster. J Comp Neurol 230: 155-67.

Spark D L (1986) Translation of sensory signals into commands for control of saccadic eye movements: role of primate superior colliculus. Physiol Rev 66: 118-171.

Saito Y, Isa T (2003) Local excitatory network and NMDA receptor activation generate a synchronous and bursting command from the superior colliculus. J Neurosci 23:5854-64.

Saito Y, Isa T (2004) Laminar specific distribution of lateral excitatory connections in the rat superior colliculus. J Neurophysiol 92: 3500-10.

Saito Y, Isa T (2005) Organization of interlaminar interactions in the rat superior colliculus. J Neurophysiol 93:2898-907.

Shimono K, Kubota D, Brucher F, Taketani M, Lynch G (2002) Asymmetrical distribution of the Schaffer projections within the apical dendrites of hippocampal field CA1. Brain Res 950:279-87.

Sparks DL (1986) Translation of sensory signals into commands for control of saccadic eye movements: role of primate superior colliculus. Physiol Rev 66:118-71.

Tardif E, Delacuisine B, Probst A, Clarke S (2005) Intrinsic connectivity of human superior colliculus. Exp Brain Res 166: 316-324.

Tsotsos JK (1992) On the relative complexity of active vs. passive visual search. Inter J Comp Vision 7: 127-141.

Trappenberg TP, Dorris MC, Munoz DP, Klein RM (2002) A model of saccade initiation based on the competitive integration of exogenous and endogenous signals in the superior colliculus. J Cogn Neurosci 13: 256-271.

Van Opstal AJ, Van Gisbergen JA (1989) Scatter in the metrics of saccades and properties of the collicular motor map. Vision Res 29:1183-96.

Van Opstal AJ, Van Gisbergen JA, Smit AC (1990) Comparison of saccades evoked by visual stimulation and collicular electrical stimulation in the alert monkey. Exp Brain Res 79:299-312.

Acknowledgements

My profound gratitude goes to Professor Tadashi Isa, my advisor, and Assistant Professor Katsuyuki Kaneda, who both contributed significantly to the work described in this thesis. Professor Isa's wide knowledge and his logical way of thinking have been of great value for me. This work would not have been possible without their supports.

I wish to express my sincere thanks to Associated Professor Boonyong and Mayuree Tantisira at Chulalongkorn University, Thailand, who introduced me to the field of neurophysiology. I also want to thanks Associated Professor Thongchai Sooksawate who taught me the patch clamp recording technique.

I am deeply grateful to Ministry of Education, Culture, Sports, Science and Technology in Japan for the scholarship that they gave me in order to study in Japan.

I wish to thank Professor William C. Halls and Psyche Lee at Duke University for their warm hospitalities while I was there for learning the photostimulating system.

I would like to thanks Dr. Ken Shimono who provided me the analytical methods for the data from MED system. I am grateful for Rika Yamazaki from Panasonic company who helped me to fix the problems of MED systems.

I would like to thank Professor Douglas Munoz and Robert Marino, at Queen's University, Canada, who gave me a lot of fruitful idea in lateral connection of the SC, especially the way of cutting the horizontal slice.

My very special thanks go to Kaoru Isa who taught me the morphological staining methods and always keep helping me in every details of my life. I also would like to thank Tomoko Katoh for her good taking care of the experimental animals. I am grateful to the secretaries in Professor Isa's group for helping me in many different ways.

Throughout this work, a number of people have contributed key ideas and criticisms. I wish to thank all members in Isa's group for all of those supports.

I wish to thank my parents and my sister Mai for always sending me their loves via telephone. Especially, I would like to give my special thanks to my husband Pop whose patient love enabled me to complete this work.